

NASA-CR-3937 19860004808

NASA Contractor Report 3937

FOR REFERENCE

NOT TO BE TAKEN FROM THIS ROOM

Magnetic Suspension and Balance System Advanced Study

R. W. Boom, Y. M. Eyssa,
G. E. McIntosh, and M. K. Abdelsalam

CONTRACT NAS1-17931
OCTOBER 1985

LANGLEY RESEARCH CENTER
LIBRARY, NASA
HAMPTON, VIRGINIA

NOV 1985

LANGLEY RESEARCH CENTER
LIBRARY, NASA
HAMPTON, VIRGINIA

NASA



NF02284

NASA Contractor Report 3937

Magnetic Suspension and Balance System Advanced Study

R. W. Boom, Y. M. Eyssa,
G. E. McIntosh, and M. K. Abdelsalam

Madison Magnetics, Inc.

Madison, Wisconsin

Prepared for
Langley Research Center
under Contract NAS1-17931

NASA
National Aeronautics
and Space Administration

**Scientific and Technical
Information Branch**

1985

FOREWORD

The purpose of this report is to present the results of an advanced study of a Magnetic Suspension and Balance System suitable for a wind tunnel having an 8 ft. x 8 ft. test section capable of operating at speeds up to Mach 0.9 with $\pm 0.1\%$ control forces at 10 Hz for an F-16 model airplane.

R. W. Boom, Y. M. Eyssa, G. E. McIntosh and M. K. Abdelsalam are the major contributors to the study.

Use of trade names or names of manufacturers in this report does not constitute an official endorsement of such products or manufacturers, either expressed or implied, by the National Aeronautics and Space Administration.



FINAL REPORT ON NASA CONTRACT NAS1-17931

"MAGNETIC SUSPENSION AND BALANCE SYSTEM ADVANCED STUDY"

PROJECT SUMMARY

The objectives of this study were to investigate advanced topics in Magnetic Suspension and Balance Systems (MSBS). The advanced topics were identified as potential improvements by Madison Magnetics, Inc. (MMI) during a 1984 study of an MSBS utilizing 14 external superconductive coils and a superconductive solenoid in the airplane test model suspended in a wind tunnel. When substituted in the 1984 MMI design, these improvements result in a selectively new 1985 MSBS design. Specifically, the objectives were to investigate test model solenoid options, dynamic force limits on the model, magnet cooling options, structure and cryogenic designs, power supply specifications, and cost and performance evaluations.

All objectives were achieved, as seen in the specification and performance chart, where each entry shows improvement for the 10 Hz \pm 0.1% force requirement.

Specifications

MMI Designs	Cost (\$10 ⁶)	System Weight (tonnes)	Coil Weight (tonnes)	Coil Conductor (MAm)	Helium Liquefier (liters/h)
1984	29.9	368	171	755	560
1985	21.4	210	80.9	468	375

Performance

MMI Designs	Test Coil Pole Strength (10 ⁴ Am)	Wing Magnetization (tesla)	AC Loss at 10 Hz to Helium (W)	Control Freq. Limit (Hz)	Magnet Stored Energy (MJ)	System Power (MW)
1984	3.75	0.70	2212	10	906	97.2
1985	4.45	0.98	522	30	408	31.2

The improvements are due to: magnetic holmium coil forms in the model, better rare earth permanent magnets in the wings, fiberglass-epoxy structure replacing stainless steel, better coil configuration and new saddle roll coil design.

Primary commercial application of the research is for high performance conventional and cryogenic wind tunnels. Secondary commercial application to other disciplines is expected for the high current density test model coil and for the low loss AC magnet designs.

TABLE OF CONTENTS

Foreword.....	iii
Project Summary.....	v
Table of Contents.....	vii
List of Figures.....	ix
List of Tables.....	x
References.....	xi
I. Introduction.....	1
I.1 Background.....	1
I.2 Summary.....	2
I.3 Phase I Accomplishments.....	4
I.3.1 Phase I Program.....	4
I.3.2 Phase I Objectives.....	5
I.3.2.1 Best Design at 4.2 K.....	5
I.3.2.2 Best Design at 1.8 K.....	5
I.3.2.3 Best Design for Forced Flow Cooling.....	5
I.3.2.4 Best Structural Design for Minimum AC Losses.....	6
I.3.2.5 Best Cryogenic Systems for Various Duty Cycles.....	6
I.3.2.6 Stable Conductor Designs with Low AC Losses.....	6
I.3.2.7 Parameter Variation vs. Control Frequency.....	7
I.3.2.8 Improved Power Supply Specifications.....	7
I.3.2.9 Series Connected Coils.....	8
I.3.2.10 Solenoid Designs for Suspended Models.....	8
I.3.2.11 Drag Coils Elimination Study.....	8
I.3.2.12 Design Summaries and Cost Estimates.....	8
I.3.2.13 Key Items for Phase II Research and Development.....	9
II. System Design.....	11
II.1 MSBS System Concepts.....	11
II.2 Magnetic Properties of the Model Coil.....	12
II.3 Wing Permanent Magnet Material.....	17
II.4 Magnetic Field Requirements.....	18
II.5 Cross Coupling.....	19
II.6 System Configuration.....	21
III. Magnet Design.....	23
III.1 Magnet System.....	23
III.1.1 Coil Shapes.....	23
III.1.2 Coil Terminal Voltages.....	23
III.1.3 Magnet Control Requirement.....	24
III.2 Conductor.....	25
III.3 Magnet System Concept.....	25
III.3.1 System Analysis.....	25
III.3.2 Model Core Solenoid.....	29
III.3.3 X, Y, Z and R Coils.....	33

IV.	System Analysis.....	39
IV.1	Parametric Study.....	39
IV.2	Conductors.....	39
	IV.2.1 Conductor for Pool Boiling.....	40
	IV.2.2 Forced Flow Cooling.....	47
IV.3	Cooling Methods.....	49
	IV.3.1 Pool Cooling at 4.2 K.....	49
	IV.3.2 Superfluid Helium at 1.8 K.....	49
	IV.3.3 Forced Flow Cooling.....	50
	IV.3.4 Conclusions.....	50
IV.4	AC Losses and Control Requirements.....	51
	IV.4.1 External Magnet Losses and Control Requirements.....	51
	IV.4.2 Model Coil Losses and Control Limits.....	52
IV.5	Drag Coil Requirements.....	54
V.	Structural and Thermal Design.....	55
V.1	Structure Concepts.....	55
V.2	Materials.....	59
V.3	Forces and Torques.....	65
V.4	Structural Design.....	65
V.5	Electrical Isolation.....	67
V.6	Weight Summary.....	68
VI.	Thermal and Cryogenic System.....	69
VI.1	Cryogenic Concepts.....	69
VI.2	Cryostat Heat Leak.....	69
VI.3	Magnet Power Leads.....	72
VI.4	Operating Losses.....	72
VI.5	Component Review.....	75
VI.6	Cryogenic System Cost Estimate.....	78
VI.7	Cooldown Analysis.....	78
VI.8	General Operating Plan.....	79
VI.9	Cryogenic Impact of 1.8 K Operation.....	81
VII.	Cost Estimate.....	83
VIII.	Appendices.....	87
A.	Appendix A Magnetic Pole Strength of a Superconducting Solenoid with Holmium Mandrel	89
B.	Appendix B Roll Torque Analysis	91
C.	Appendix C Forces and Torque Requirements	95
D.	Appendix D Cross Coupling Analysis	97
E.	Appendix E Optimizations of Drag and Roll Coils	101
F.	Appendix F Tunnel Wall Constraints	111

LIST OF FIGURES

Figure II.1	1984 Magnet System.....	13
Figure II.2	1985 Magnet System with Saddle Roll Coils and In-Line Drag Coils.....	14
Figure II.3	Demagnetization Curve of $Nd_{13.5}Dy_{1.4}Fe_{77}B_8$ Sintered Magnet.....	18
Figure III.1	Core Magnet Cryostat.....	34
Figure IV.1	Z or Y Coil Parameters vs. Gross Current Density J.	43
Figure IV.2	Z or Y Coil Outer Radius vs. Magnetic Field.....	44
Figure IV.3	Cryostable 11 kA AC Cable.....	45
Figure IV.4	15 kA Forced Flow Conductor.....	48
Figure V.1	Cryostat Longitudinal Section.....	56
Figure V.2	Cryostat Transverse Section.....	57
Figure V.3	Structural Electric Break.....	60
Figure V.4	Cold Shell Electrical Break.....	61
Figure V.5	Egg Crate Electrical Break.....	62
Figure V.6	End Plate Assembly.....	63
Figure V.7	Roll Coil Restraint and Structural Stiffener.....	64
Figure VI.1	MSBS Cryogenic Schematic.....	70
Figure B.1	F16 Wing.....	92
Figure B.2	Wing Cross-Sectional Area.....	93
Figure E.1	Field Due to Current Sheet.....	102
Figure E.2	Quadrupole Field of the Roll Coil at the Model Wing Tip.....	104
Figure E.3	Field on the Axis of the X Drag Coils.....	104

LIST OF TABLES

Table II-1	Madison Magnetics MSBS 1984 and 1985 Designs.....	12
Table II-2	Holmium Magnetization vs. Applied Field at 4.2 K...	16
Table II-3	Model Coil Specifications.....	16
Table II-4	Magnetic Properties of $Nd_{15}Fe_{77}B_8$ Magnetic Material.....	17
Table II-5	Field Requirements in Tesla at Model Coil Pole Tips	19
Table II-6	X, Y and Z Coil Fields in Tesla at Zero Angle of Pitch, Yaw and Roll.....	20
Table III-1	Voltage and Power Requirements per Coil.....	24
Table III-2	Maximum Fields in Coils in Tesla.....	26
Table III-3	Forces and Torques on Z, Y and X Coils.....	26
Table III-4	Forces on the R-Coil.....	27
Table III-5	Inductance Matrix in Milli-Henries.....	28
Table III-6	Forces and Torques on the Drag Coils due to the Roll Coils.....	29
Table III-7	Model Coil Parameters.....	30
Table III-8	X Drag Coil Parameters.....	33
Table III-9	Z or Y Coil Parameters.....	35
Table III-10	Roll Coil Specifications.....	35
Table III-11	Coil Weights, kg.....	36
Table III-12	Coil AC Losses at 10 Hz.....	37
Table III-13	Eddy Current Losses in Structure and Helium Vessel.	37
Table IV-1	Z Coil Dimensions as Function of Field and Gross Current Density ($J = 1500 \text{ A/cm}^2$).....	40
Table IV-2	Z Coil Dimensions as Function of Field and Gross Current Density ($J = 2500 \text{ A/cm}^2$).....	41
Table IV-3	Z Coil Dimensions as Function of Field and Gross Current Density ($J = 3500 \text{ A/cm}^2$).....	42
Table IV-4	Z Coil Dimensions as Function of Field and Gross Current Density ($J = 4500 \text{ A/cm}^2$).....	42
Table IV-5	Characteristics of the ANL Cable Conductor.....	45
Table IV-6	ANL Cable Conductor for 4.2 K and 1.8 K Operation..	47
Table IV-7	JAERI JF-15 Forced Flow Conductor.....	49
Table IV-8	MSBS Cost Differences for 1.8 K HeII or Forced Cooling Systems Compared to 4.2 Cooling.....	51
Table IV-9	Maximum Control Variation of Current vs. Control Frequency.....	52
Table IV-10	Model Coil Losses vs. Control Requirements.....	53
Table V-1	MSBS System Estimated Weights.....	68
Table VI-1	Static Heat Leak and Cryogen Consumption.....	71
Table VI-2	Predicted Lead Losses.....	72
Table VI-3	Magnet and Cryostat Operating Losses.....	73
Table VI-4	Components of MSBS Cryogenic Systems.....	75
Table VI-5	Cryogenic System Cost Estimates.....	79
Table VII-1	MSBS Cost Estimate--Control Based on $0.1\% I_{\text{max}}$ at 10 Hz in All Coils Simultaneously.....	85
Table C-1	MSBS Requirements, 8' x 8' Test Section.....	96
Table F-1	Time Constants for Field Diffusion Through Dewar Walls.....	112

REFERENCES

- [1] H. L. Bloom et al., "Design Concepts and Cost Studies for Magnetic Suspension and Balance Systems," NASA CR-165917, July 1982.
- [2] R. W. Boom, Y. M. Eyssa, G. E. McIntosh, and M. K. Abdelsalam, "Magnetic Suspension and Balance System Study," NASA CR-3802, July 1984.
- [3] S. J. Sackett, "EFFI: A Code for Calculating the Electromagnetic Field and Inductance in Coil Systems of Arbitrary Geometry," Lawrence Livermore Laboratory, Livermore, California, UCRL-52402, March 1978.
- [4] V. Takashi et al., "Development of a 30-kA Cable-in-Conduit Conductor for Pulsed Poloidal Coils," IEEE Transaction on Magnetics, Vol. MAG-19, No. 3, May 1983, p. 386.
- [5] W. Schauer and F. Arendt, "Field Enhancement in Superconducting Solenoids by Holmium Flux Concentrators," Cryogenics, October 1983.
- [6] R. W. Hoard et al., "Field Enhancement of a 12.5 T Magnet Using Holmium Poles," IEEE Transactions on Magnetics, Vol. MAG-21, No. 2, March 1985.
- [7] M. Sagawa et al., "Permanent Magnet Materials Based on the Rare Earth-Iron-Boron Tetragonal Compounds," IEEE Transactions on Magnetics, Vol. MAG-20, No. 5, September 1984.
- [8] S. Arai and T. Shibata, "Highly Heat Resistant Nd-Fe-Co-B System Permanent Magnets," paper presented at the 1985 INTERMAG Conference, St. Paul, Minnesota.
- [9] S. H. Kim, S. T. Wang, and M. Lieberg, "Operating Characteristics of a 1.5 MJ Pulsed Superconducting Coil," Advances in Cryogenic Engineering, Vol. 25, Plenum Press, N.Y., 1980, pp. 90-97.



I. INTRODUCTION

I.1. Background

Magnetic suspension and balance systems (MSBS) for wind tunnels have been increasingly developed and utilized during the past 25 years. The primary aerodynamic advantage of MSBS is the elimination of air flow disturbances caused by the test model mechanical support system and by the required alterations in the test model. The primary technological advantages of MSBS are that static and dynamic forces and torques on the test model can be applied and recorded (from magnet currents) without the severe sting restraints.

The potential availability of MSBS for large transonic tunnels improves steadily in line with the expanding broad utilization of superconductive magnet systems in many fields, such as: magnetic resonance imaging, high energy physics, fusion, and energy storage. Superconductive systems are needed because the external magnets are far from the test model and, in some cases, tend to cancel fields from other magnets.

The recent conceptual design studies by General Electric [1] in 1981 and by Madison Magnetics [2] in 1984 show that practical superconductive MSBS systems can be built well within the present state of the art for superconductive systems. Design improvements and cost reductions continue in this third design study for a MSBS suitable for an 8' x 8' test section at Mach 0.9 with $\pm 0.1\%$ control forces at 10 Hz for an F16 model airplane.

I.2. Summary

The cost estimate for this MSBS design is \$21,398,000 in 1985 dollars, which is a reduction of 29% from the 1984 Madison Magnetics, Inc. (MMI) design. The 1984 design was itself a considerable improvement over the 1981 design due, primarily, to the efficient compact mounting of external magnets in one dewar so as to be as close as possible to the test airplane model in the wind tunnel.

Some special features of the MMI-1984 design are as follows:

- * Superconductive persistent solenoid in the suspended airplane model instead of magnetized iron.
- * Permanent magnet wings instead of magnetized iron wings.
- * New race-track roll coils.

The new features of the MMI-1985 design are:

- * Magnetic holmium coil forms for the test model superconducting core solenoid.
- * Better permanent magnet material, $\text{Nd}_{15}\text{Fe}_{77}\text{B}_8$, in the wings.
- * Saddle roll coils and in-line smaller diameter drag coils.
- * Fiberglass epoxy structure.

In Chapter II, System Design, the system specifications are given for both 1984 and 1985 MMI designs. The reduction in ampere-meters for 1985 is about 38%. The properties of the holmium test model winding core and of the $\text{Nd}_{15}\text{Fe}_{77}\text{B}_8$ magnetic boron rare earth wing material are given. Field requirements and cross-coupling effects are determined for optimized coil locations.

In Chapter III, Magnet Design, the specifications for the X, Y, Z and R coils are given. AC losses are dominated by hysteresis losses at 10 Hz in the NbTi filaments. The structure is mostly large plates of

fiberglass-epoxy which have no AC loss. The EFFI code [3] modified by University of Wisconsin is used to find stored energy and mutual forces between magnets. Operational possibilities for current (and force) directions in the coils determine force extremes on the structure, as described.

In Chapter IV, System Analysis, a detailed comparison is made between magnets cooled in helium baths at 4.2 K and 1.8 K and cooled by forced flow supercritical helium above 5.2 K. The 4.2 K bath cooling is shown to be most economical. The 1.8 K bath cooling option is potentially attractive for intermittent short-run time use, which is not the operational specification for this study. Forced flow cooling has very large helium pumping losses and is third choice.

Eliminating both drag coils is shown to be impossible. Operation with one drag coil is possible but only at the cost of more system ampere-meters of conductor.

In Chapter V, Structural and Thermal Design, a new fiberglass-epoxy structure is described. This non-metallic lightweight structure has no AC losses, which would have eliminated the major loss in the 1984 design. The common objection to using fiberglass-epoxy is helium leakage which does not apply here since the epoxy structure is totally immersed inside the helium bath. Electrical eddy current losses are minimized by electrical breaks in key metallic structural loops. The overall MSBS weight, components plus structure, is about 60% that of the 1984 design.

In Chapter VI, Thermal and Cryogenic System, the smaller heat load of this MSBS design needs a 375 ℓ /h helium liquefier as compared to 560 ℓ /h in the 1984 design. The cryogenic system cost is reduced by 15%. A brief discussion of advantages and disadvantages of a 1.8 K system is given.

In Chapter VII, Cost Estimate, the MSBS cost estimate is \$21,398,000. Compared to the 1984 design [2], major reductions are achieved in: 1.3.2 (winding machine construction) due to available commercial equipment; 1.3.9 (power supplies) due to smaller magnets; 1.3.12 (support structure) due to simpler fiberglass-epoxy structure slabs; 1.3.18 (manufacturing checkout) due to simpler system; and all magnet construction (1.3.3, 1.3.4, 1.3.5, 1.3.6 and 1.3.7) due to smaller, simpler coils.

In Chapter VIII, Appendices, six sections provide background derivations and calculations for model magnet pole strengths, roll torques, force requirements, cross coupling, drag and roll coil optimization and tunnel wall thickness constraints.

I.3. Phase I Accomplishments

I.3.1. Phase I Program

The objectives of this Phase I study are to investigate advanced topics in the design of MSBS with emphasis in the superconductive magnet design area. Many potential improvements and variations noticed by MMI during the 1984 design are the advanced topics considered.

The objectives are listed below with short descriptive answers and with reference to the longer, more detailed discussion in the main report. We choose to present the sum effect of the improvements as an integrated new MSBS design, which is in fact our 1984 design with these improvements. The interaction of changes with the whole MSBS requires a system design evaluation. Therefore, the result of the study of the advanced topics is a selectively new 1985 design.

I.3.2. Phase I Objectives

I.3.2.1. Best Design at 4.2 K

Open pool cooling in 4.2 K-one atmosphere helium in one large dewar for all 14 external solenoids and roll coils is the best design and is the cooling option of this report. Chapter IV, Section IV.2 through IV.2.1.1, Section IV.3.1, and Table IV-6 all support this choice with cost and performance benefits.

I.3.2.2. Best Design at 1.8 K

Open pool cooling in superfluid helium at 1.8 K-one atmosphere is the second best choice. Conductor cooling is better than at 4.2 K, the amount of conductor is \$750,000 less, and the added cost of 1.8 K refrigeration is about \$1,500,000. Thus, an 1.8 K system is more expensive by 3.5% of the $\$21 \times 10^6$ system cost. This option is described in IV.2.1.2, IV.3.2 and IV.3.4.

In IV.9 a zero cost 1.8 K option is seen to provide several hours of daily operation, which might be adequate for a tunnel with long model change times. Several hours is less than the specified 2h at full load and 8h at 1/4 load per day.

I.3.2.3. Best Design for Forced Flow Cooling

Using one of the best forced flow conductors, the J15 conductor developed at JAERI in Japan [4], the optimized design for MSBS is a 15 kA conductor. The helium flow work in all 14 magnets is 1500 W, which is much larger than the total 918 W at full load at 4.2 K. The added MSBS system cost increase is only 1.6%. This forced flow option is considered less stable and is the third choice.

Forced flow cooling is described in IV.2.2, IV.3.3 and IV.3.4.

I.3.2.4. Best Structural Design for Minimum AC Losses

Epoxy-fiberglass structural slabs, longitudinal electrical breaks in the inner and outer cold walls of the cryostat, and radial breaks in the end plate/drag coil containment assemblies all combine to reduce full load AC structure losses to 200 W (from 1560 W). This eliminates the largest previous loss. The breaks utilize sharp triangular ridges which bite into a Vespel sealing strip. Sections V.1 and V.5 and Figs. V.3, V.4 and V.5 cover the loss aspects of this structural design.

I.3.2.5. Best Cryogenic Systems for Various Duty Cycles

The specified duty cycle of 2h at full load, 8h at 1/4 load and 14h at zero load is best met by sizing the refrigeration system for the average daily load and then meeting the peak load with extra stored helium for the 4.2 K and forced flow options. For 1.8 K superfluid cooling the enthalpy of 1.8 K helium raised in temperature to 2.0 K during peak loads applies the same flywheel averaging effect to the liquefier size. This "average" size is calculated explicitly in VI.4 and used in VI.9.

I.3.2.6. Stable Conductor Designs with Low AC Losses

Sections IV.1 through IV.2.1.2 present a comprehensive analysis of the ANL-11 kA conductor [8] for MSBS stable low loss use in 4.2 K or 1.8 K pool cooling. The conductor, pictured in Fig. IV.3, is subject to a maximum field change of 0.4 T/s although it can withstand 11 T/s and remain superconducting. The remaining concern, the AC losses, are primarily NbTi hysteresis losses which constitute the major cryogenic loss at full load. The ANL conductor is a completely verified AC pulsed conductor ideally suited for MSBS use.

The forced flow conductor, IV.2.2, is less interesting because of its smaller stability margin. Total losses including AC losses are less than the helium pumping losses at low temperature.

I.3.2.7. Parameter Variation vs. Control Frequency

In Section IV.4 it is shown that the product $[\Delta I f]_{\max} \leq 16$ for $B < 6T$ and $\dot{B} < 6 T/s$ in the 14 external magnets. $\pm \Delta I\%$ is the variation in current in any coil at control frequency f . The model coil limit is $[\Delta I f]_{\max} \leq 3$. Thus the product control frequency times AC force amplitude can be increased by a factor of 3 from the $\pm 0.1\%$ force at 10 Hz without significant losses in either the model coil or the 14 external coils.

I.3.2.8. Improved Power Supply Specifications

The requirement for dynamic control is $\pm 0.1\%$ of any magnet current at 10 Hz. Accordingly, the maximum voltage across any MSBS coil is set to satisfy this requirement. The inductances used to calculate voltages are the self inductance of each coil, since the inductive mutual coupling between the different sets of coils is very small. The extra coil groups (X, Y, Z and R) are accounted for in the values of self inductances used.

The R coils are the primary source of mutual inductive coupling and induced voltages V_p . By operating these coils in series with one power supply many unwanted high voltage options are eliminated. Thus the voltages required are reduced and the total installed power is now 31.2 MW. Smaller coils also contribute to less required power.

Section III.1.2 covers the power supply specifications in detail.

I.3.2.9. Series Connected Coils

As described in the previous section the R coils are connected in series. All other coils are individually powered for maximum freedom of control.

I.3.2.10. Solenoid Designs for Suspended Models

The new design feature is the magnetic holmium core which contributes an 18.7% increase to the model solenoid pole strength (see Section III.3.2). This change reduces the size of the X and Z coils by 18.7%.

I.3.2.11. Drag Coils Elimination Study

In IV.5 an analytic proof is presented which shows that one drag coil is required. The present design of two symmetrical drag coils is more efficient.

I.3.2.12. Design Summaries and Cost Estimates

The cost estimate given in Section VII.1 of \$21,398,000 reflects the smaller magnet system due to a higher pole strength test model solenoid, the more efficient saddle roll coils, and the new permanent magnet material $\text{Nd}_{15}\text{Fe}_{77}\text{B}_8$ in the wings. A discussion of the cost logic is given in Section VII. Costs for checkout and acceptance testing, position sensors and control systems are taken from NASA CR-165917 for Case 1, Alternate G [1].

Design summaries are:

1. Model coil.....Table III-7
2. X drag coil.....Table III-8
3. Z or Y coil.....Table III-9
4. Roll coils.....Table III-10
5. Coil weights.....Table III-11
6. Cryogenic system.....Table VI-4
7. Structure.....Chapter V

I.3.2.13. Key Items for Phase II Research and Development

1. Model coil construction and test of a full-scale dewar and coil wound on a holmium coil form is the most important task. The current density should achieve the 30 kA/cm² used in this design and the coil should survive 10 Hz mechanical oscillations within the prescribed angular limits for pitch, yaw and roll. The coil should remain superconducting and the helium boil-off rate should be acceptable. This confirmation research and development would substantiate MSBS system feasibility.

2. A model coil program for 60 kA/cm² solenoids should be initiated. Although this is perceived to be an upper limit for current density in these conditions, it is felt to be so important that an upper limit of J_c should be established. At 60 kA/cm² all magnets except roll and Y coils could be greatly reduced in size.

3. A model wing of Nd₁₅Fe₇₇B₈ should be fabricated and tested to confirm utility and to determine if the 15% stainless steel structure skin is necessary.

4. New MSBS system designs should be continued. The major advances in this present study were not predicted. The expectation is that other improvements are possible. Cost reductions are certainly available in case less stringent duty cycles are acceptable. The 2-hour, $\pm 0.1\%$ force at 10 Hz requirement determines cryogenic system and power supply specifications. For a shorter duty cycle the 1.8 K operation is very attractive (Section VI.9).

II. SYSTEM DESIGN

II.1. MSBS System Concepts

The 1984 MSBS [2] design by MMI included design improvements which reduced the costs to 30% of previous estimates. The major improvements for the 1984 system sketched in Fig. II.1 are:

- * A 70 cm long potted persistent superconducting solenoidal coil, 11.5 cm O.D., and 6.1 tesla is the model core. A superconducting coil produces higher magnetic moments and pole strengths than a magnetized iron core or a permanent magnet core.
- * The model wings contain permanent magnets that occupy 85 percent of the wing volume. The rest of the wing volume is high strength stainless steel.
- * Z and Y gradient coils in Fig. II.1 are symmetric arrays of four solenoid magnets. They are bipolar coils to control and manipulate the model. The conductor for all coil systems is the 11-kA low-loss cryostable conductor.
- * The drag coils to counterbalance wind drag forces are large diameter solenoids.
- * The roll coils are four race-track coils optimized for minimum ampere-meters.

The 1985 MSBS design by MMI adds four additional improvements:

1. The use of a holmium coil mandrel in the suspended model to increase the core pole tip magnetic moment by 18.7% from 3.75×10^4 Am to 4.45×10^4 Am.
2. The use of a new permanent magnet material $\text{Nd}_{15}\text{Fe}_{77}\text{B}_8$ in the

suspended model wings which reduces the external roll magnet size by about 25%.

3. The new arrangement for roll and drag coils shown in Fig. II.2 provides a more economical and compact design.
4. The use of fiberglass-epoxy slabs as the principal structure to reduce AC losses.

These four improvements reduce significantly the ampere-meters and energy stored in all 14 external magnets. Table II-1 compares the two MMI designs.

Table II-1

Madison Magnetics MSBS 1984 and 1985 Designs

Coils	X	Y	Z	R	Total
1984 design					
Ampere-meters (MAm)	362	100*	86	207	755
Energy stored (MJ)	656	60	50	140	906
1985 design					
Ampere-meters (MAm)	172	71**	71	154	468
Energy stored (MJ)	216	38	38	116	408

*The Y coils in the 1984 design were undersized due to error in cross coupling relations.

**Actual ampere-meters needed for Y coils are 63 MAm. For simplicity of design and to have a complete symmetry, the Y coils are sized the same as the Z coils.

The ampere-meters of conductor in the 1985 design decrease to 62% and the stored energy decreases to 45% of the 1983 design.

II.2. Magnetic Properties of the Model Coil

The model core solenoid is an epoxy impregnated coil with gross current density of 30 kA/cm^2 at 6.1 tesla maximum fields. Such coils do

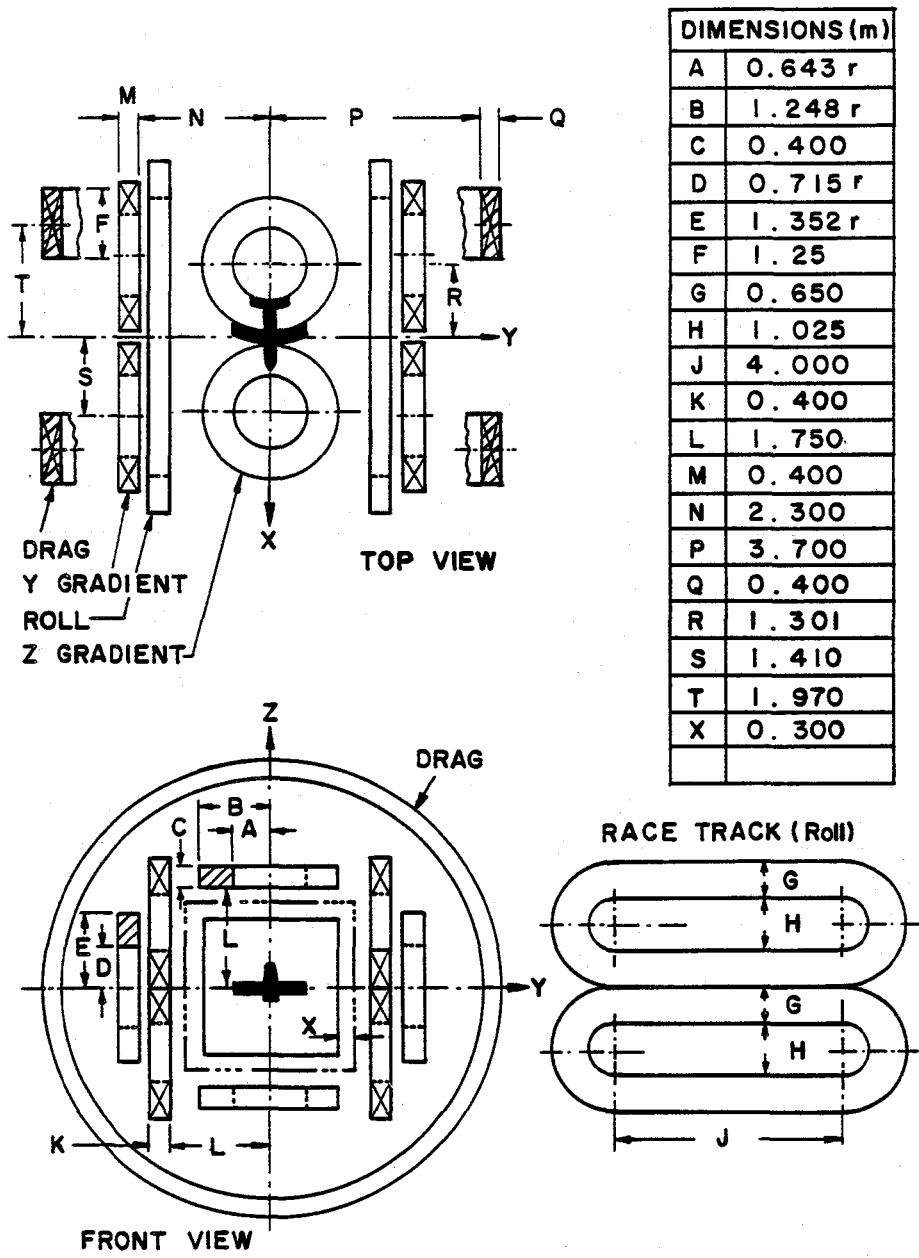


Figure II.1. 1984 Magnet System

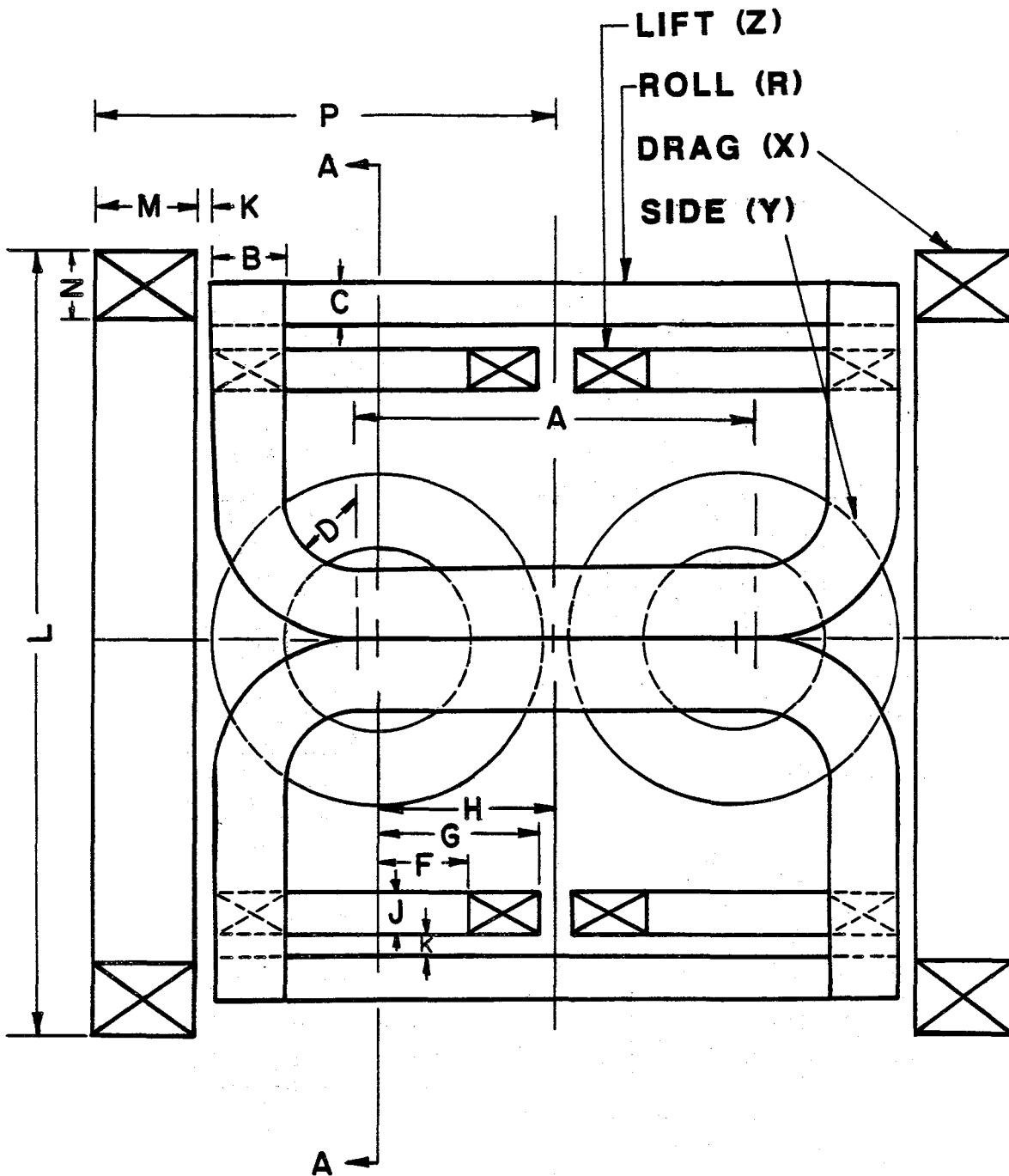
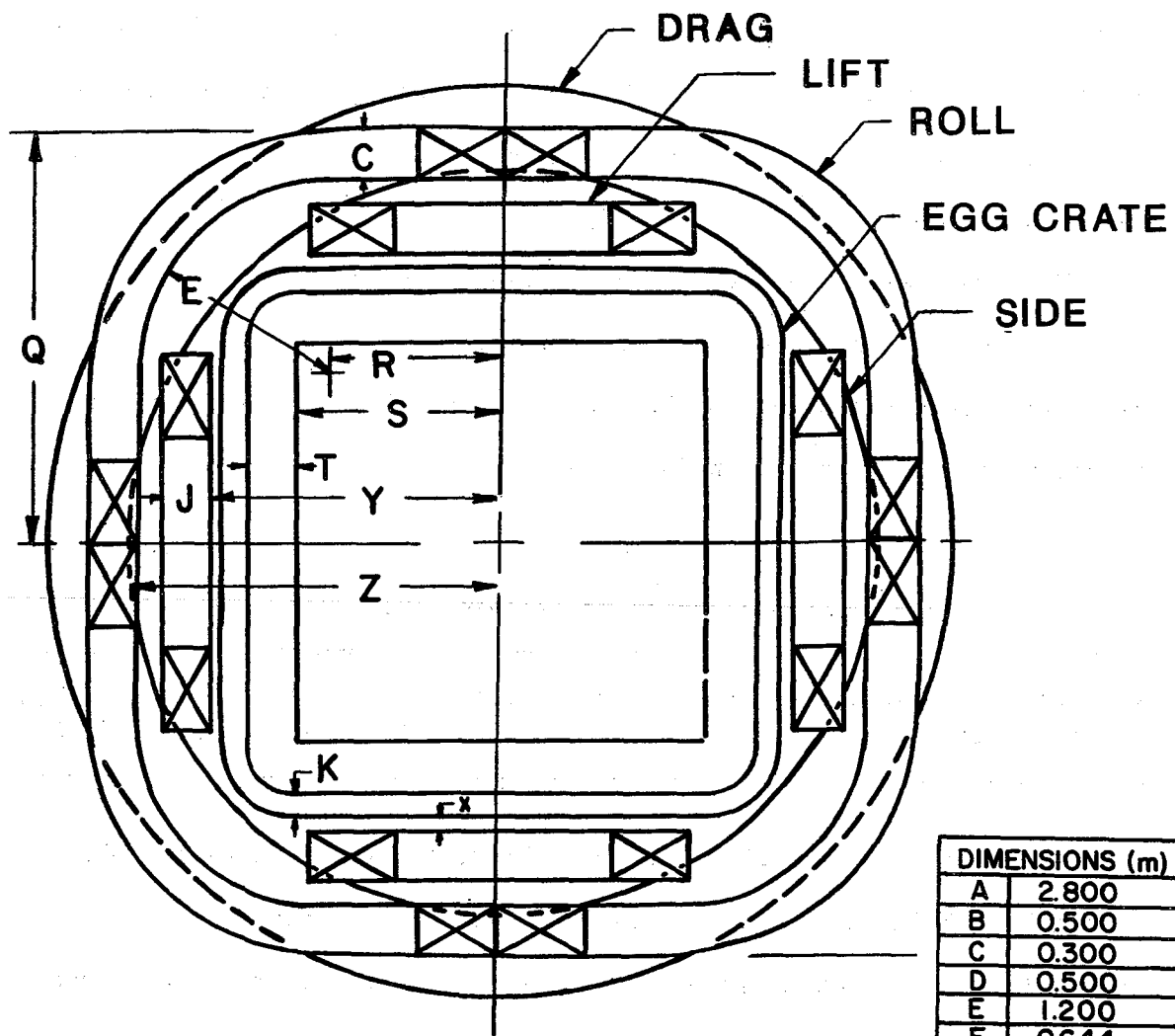


Figure II.2. 1985 Magnet system with saddle roll coils and in-line drag coils.



VIEW A-A

DIMENSIONS (m)	
A	2.800
B	0.500
C	0.300
D	0.500
E	1.200
F	0.644
G	1.153
H	1.250
J	0.300
K	0.152
L	5.514
M	0.700
N	0.500
P	3.252
Q	2.505
R	1.005
S	1.219
T	0.305
X	0.076
Y	1.753
Z	2.205

Figure II.2 (continued)

not contain much copper or cooled surfaces, and their ability to tolerate disturbances is limited to the adiabatic heat capacity of the conductor material. However, the absence of large amounts of copper and helium in the windings allows such coils to operate at current densities up to ten times as large as those for cryostable coils, which is ideal for model cores.

The improvement in the present design comes from the holmium mandrel. Holmium has superior magnetic properties at 4.2 K with a saturation magnetic moment of 3.9 tesla. Table II-2 lists the magnetization of holmium at 4.2 K [5,6].

Table II-2
Holmium Magnetization vs. Applied Field at 4.2 K

Magnetization force (T)	0	0.1	0.52	1.0	1.5	2.5	3.5	4.5	6.5
Magnetization (T)	0	1.6	2.48	2.9	2.98	3.12	3.25	3.35	3.7

With the specifications shown in Table II-3, the total magnetic pole strength of holmium and winding is 4.45×10^4 Am. Appendix A details calculation of the magnetic pole strength as a function of winding and holmium dimensions.

Table II-3
Model Coil Specifications

	ID (cm)	OD (cm)	Length (cm)	Weight (kg)	Magnetic Pole Strength (Am)
Winding	8.26	11.5	70	26.8	3.75×10^4
Mandrel	6.14	8.26	70	<u>14.5</u>	<u>0.70×10^4</u>
Total				41.3	4.45×10^4

Eddy current losses in the model coil are mainly hysteresis losses in the superconductor filaments. For two micron filaments, the expected hysteresis loss is 0.046 watt (4.6×10^{-3} J/cycle) with $\pm 0.1\%$ field variation at 10 Hz for all X, Y, Z and roll coils at full current. The holmium mandrel resistivity of 3×10^{-8} Ωm at 4.2 K results in eddy current losses of about 6.4×10^{-4} watts under the same 10 Hz current control conditions or two orders of magnitude less than the superconductor hysteresis loss.

II.3. Wing Permanent Magnet Material

A new superior permanent magnet material $\text{Nd}_{15}\text{Fe}_{77}\text{B}_8$ is planned for the wings [7,8]. The magnetic properties are listed in Table II-4.

Table II-4

Magnetic Properties of $\text{Nd}_{15}\text{Fe}_{77}\text{B}_8$ Magnetic Material

	Br (T)	Hc (kA/m)	(BH)max (kJ/m ³)	Tc (K)
$\text{Nd}_{15}\text{Fe}_{77}\text{B}_8$	1.23	960	290	585
$\text{Nd}_{15}(\text{Fe}_{0.9}\text{Co}_{0.1})_{77}\text{B}_8$	1.23	800	290	671
$\text{Nd}_{15}(\text{Fe}_{0.8}\text{Co}_{0.2})_{77}\text{B}_8$	1.21	820	260	740

As shown in Fig. II-3, the new permanent magnet material has large values of M_r (residual magnetism) and H_c (demagnetization critical field). M_r stays well above 1.2 tesla for most of the demagnetizing field and well over 1.15 up to $H_c = 9.60$ kA/m (1.21 tesla). With $M_r = 1.15$ tesla and 85% wing volume, the average magnetization in the wing is 0.9775 tesla. The required applied B_z field from the roll coil at the

tip of the wings at zero angle of roll is $B_z = 0.235$ tesla compared to 0.308 tesla used in the previous design (pp. 111-14 of Ref. 2), which is based on average magnetization of 0.7 tesla using SmCo_5 permanent magnet material. Elimination of the stainless steel skin support in the wing increases the permanent magnet wing volume to 100% and the average magnetization to 1.12 tesla. This reduces the B_z roll field to 0.205 tesla and reduces the roll field A_m by 12.7%. Mathematical relations between the roll field required at the wing tips and the average magnetization are in Appendix B.

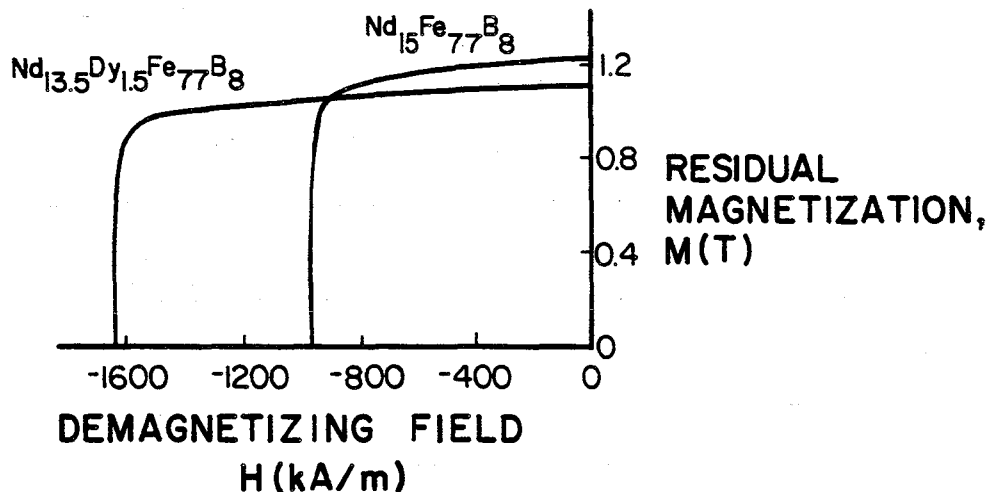


Figure II.3. Demagnetization curve of $\text{Nd}_{13.5}\text{Dy}_{1.5}\text{Fe}_{77}\text{B}_8$ sintered magnet [5].

II.4. Magnetic Field Requirements

Maximum external field requirements at the model pole tips during maximum pitch and yaw are listed in Table II-5 for the above

improvements in model and wing magnetic material. These fields determine the size of the 14 external magnets. Appendix C lists the force and torque requirements and their relation to the external magnets' field.

Table II-5

Field Requirements* in Tesla at Model Coil Pole Tips

	Lift	Lateral	Drag	Roll	
				(15% SS in Wings)	No SS
Field component*	B_z	B_y	B_x	B_{ZR}	
Field location**	$\alpha = 30^\circ$ $\beta = 10^\circ$	$\alpha = 30^\circ$ $\beta = 10^\circ$	$\alpha = 30^\circ$ $\beta = 10^\circ$	$\phi = 0$ zero roll	
Field required to produce force	0.110	0.0155	0.0469	-	-
Field required to produce torque	0.0155	0.0045	-	0.235	0.205
Total field	0.1255	0.02	0.0469	0.235	0.205
Margin for control	2%	2%	2%	2%	2%
Total field required	0.128	0.0205	0.048	0.24	0.208

*Fields B_x , B_y , B_z and B_{ZR} are fields required to produce maximum forces and torques at maximum angles of pitch, yaw and roll. These fields are produced by all four coil systems collectively.

** α is the pitch angle, β is the yaw angle, and ϕ is the roll angle.

II.5. Cross Coupling

The discussion detailed in Appendix D covers all first order cross couplings between X, Y, Z, and R coils during pitching, yawing, and rolling. There were some mistakes regarding signs in some of the

equations and the cross-coupling matrix (e.g., Equations 111.9 and 111.10) in Ref. 2. The correct equations and matrix are:

Equation II.1

$$\begin{aligned}
 B_x &= (\cos \alpha \cos \beta) B_{x_0} - (\sin \beta) B_{y_0} - (\sin \alpha) B_{z_0} \\
 B_y &= (1/2 \sin \beta) B_{x_0} + (\cos \alpha \cos \beta) B_{y_0} + (0) B_{z_0} - A \sin \alpha \\
 B_z &= (1/2 \sin \alpha) B_{x_0} + (0) B_{y_0} + \cos \alpha \cos \beta B_{z_0} - A \sin \beta
 \end{aligned}$$

Equation II.2

$$\begin{bmatrix} \cos \alpha \cos \beta & -\sin \beta & -\sin \alpha \\ \frac{\sin \beta}{2} & \cos \alpha \cos \beta & 0 \\ \frac{\sin \alpha}{2} & 0 & \cos \alpha \cos \beta \end{bmatrix} \begin{bmatrix} B_{x_0} \\ B_{y_0} \\ B_{z_0} \end{bmatrix} = \begin{bmatrix} B_x \\ B_y + A \sin \alpha \\ B_z + A \sin \beta \end{bmatrix}$$

A = (roll coil field, B_{ZR})x L/2b where L is the core length and 2b is the wing span. B_{x_0} , B_{y_0} , and B_{z_0} are the X, Y, Z coil fields at

zero angles of pitch and yaw. The maximum design fields of

B_{x_0} , B_{y_0} , and B_{z_0} are listed in Table II.6.

Table II-6

X, Y, and Z Coil Fields in Tesla at Zero Angle of Pitch, Yaw and Roll

	B_{x_0}	B_{y_0}	B_{z_0}	B_{ZR}
Case I (S.S.reinforced wing)	0.1664	0.1275	0.1435	0.240
Case II (no S.S.)	0.1602	0.1099	0.1390	0.204

II.6. System Configuration

The magnet system configuration for the 8' x 8' test section presented here (Fig. II.2), is similar to that presented in Ref. 2 (Fig. II.1), except for:

1. The model core has a holmium mandrel.
2. The four flat race track roll coils in Fig. II.1 are replaced by four saddle coils connected in series as shown in Fig. II-2. The new configuration reduces significantly the R coil ampere-meters required to produce a roll field of 0.24 tesla at the wing tips.
3. The two X (drag) coils are placed more in line with the Z and Y coil systems as shown to simplify the structure required to take the coupling forces between coils. This arrangement requires slightly more ampere-meters in the X coils compared to the optimum position around the four R, Y, and Z coils. However, the present arrangement simplifies the cryostat and structure design. Optimization of the drag (X), and roll (R) coil arrangement is detailed in Appendix E.

III. MAGNET DESIGN

III.1. Magnet System Requirement

The magnet system consists of one epoxy impregnated superconducting model coil with holmium mandrel, 4 Z gradient coils, 4 Y gradient coils, 2 X drag coils, and 4 R roll saddle coils. The Z, Y, and R coils are fully bipolar while the X coils are monopolar. The symmetry of the coil array enhances the reliability of the magnet system.

III.1. Magnet System Requirement

All system requirements for static forces and torques plus the 10 Hz dynamic control forces are met with the system configuration described in Chapter II. Other magnet requirements such as peak magnetic field strength, peak voltage at the magnet terminals and the structure requirements are within the state of the art.

III.1.1. Coil Shapes

All coils are solenoids except the saddle R coils. The use of saddle R coils instead of race track R coils or solenoids minimizes ampere-meters and stored energy.

III.1.2. Coil Terminal Voltages

The requirement for dynamic control is $\pm 0.1\%$ of any magnet current at 10 Hz. Accordingly the maximum voltage across any single MSBS coil is about 830 V on the X coil.

The power supply maximum voltage and power is determined for $I = 11$ kA in all coils and for the 10 Hz correction to be applied to each coil

continuously at maximum amplitude. The requirements on power supplies for initial charging to full current in all coils is less than for the 10 Hz load providing the charge time exceeds 25 sec. The 2 min charging powers are smaller, as seen in Table III-1.

Table III-1
Voltage and Power Requirements per Coil

Coil	10 Hz at 0.1% of max current		2 min charge specification	
	Voltage	Power	Voltage	Power
	V	MW	V	MW
Z	76	0.84	16.0	0.18
Y	76	0.84	16.0	0.18
X	830	9.13	174.3	1.92
R*	840	9.23	176.4	1.94
Total Power**	31.2 MW		7.22 MW	

*The four saddle coils used for roll are operated in series and are considered as one coil.

**For all coils simultaneously.

III.1.3. Magnet Control Requirement

The control requirement is $\pm 0.1\%$ of the static forces at 10 Hz. Each R, Y and Z magnet has a 3-phase Graetz bridge SCR bipolar power supply with voltages sufficient to provide the 10 Hz current variation for control (see Table III-1). The X coils are monopolar and require only monopolar power supplies. In all cases the power supply voltage must be sufficient to overcome any unwanted voltage pickup from any other coil undergoing control current correction in addition to providing its own di/dt .

III.2. Conductor

The conductor used in all X, Y, Z and R coils is the ANL 11 kA cable conductor discussed in Chapter IV.

III.3. Magnet System Concept

The magnet system configuration is shown in Fig. II.2. The system consists of 14 superconducting coils arranged around the tunnel test section. The function and arrangement of these coils is discussed in Chapter II. All the coil forms are slotted stainless steel with epoxy plate reinforcement. The forces and torques between the coils are contained by cold non-metallic structure to minimize eddy current losses. Details of the dewar and structure are in Chapters V and VI.

III.3.1. System Analysis

The computer code EFFI is used to calculate magnetic fields, forces, torques, field profiles in the tunnel area, and coil inductances.

The maximum field in each coil is found by field scanning the coil with operationally paired coils powered to ± 11 kA. The maximum values for self and total fields are listed in Table III-2. It is seen that 5.02 T on the Y and Z coils is maximum.

The homogeneity of the magnetic fields in the model region is examined in detail. Cross coupling between the different coils at different modes of operation is accounted for, as explained in Chapter II.

Table III-2

Maximum Fields in Coils in Tesla

Coil	Self Field Maximum	Total Field Maximum
R	2.94 T	4.05 T
X	4.3	4.77
Y	4.0	5.02
Z	4.0	5.02

Magnetic forces are calculated for all coils in the system under maximum static forces and moments for different modes of operation. Tables III-3 and III-4 summarize the results of these calculations. The analysis shows the need for rigid, bi-directional coil supports.

Table III-3

Forces and Torques on Z, Y and X coils

Coil	F_x MN	F_y MN	F_z MN	T_x MN·m	T_y MN·m	T_z MN·m
Z	± 3.62	± 12.05	± 2.58	± 5.69	± 7.66	0
Y	± 3.62	± 2.58	± 12.05	± 5.69	0	± 7.66
X	± 3.05	± 4.14	± 4.14	0	± 6.04	± 6.04

Table III-4

Forces on the R-Coil (half of the top left coil)

Section	Type	Axis	Length	F_x MN	F_y MN	F_z MN
1	Straight	x-axis	0.7 m	0	± 1.14	± 6.25
2	Straight	x-axis	0.7 m	0	± 0.98	± 4.23
3	Straight	x-axis	0.7 m	0	± 0.98	± 4.23
4	Straight	x-axis	0.7 m	0	± 1.14	± 6.25
5	Arc	y-axis	90°	± 4.93	± 2.00	± 6.15
6	Arc	x-axis	90°	± 9.97	± 1.94	± 1.43
7	Arc	z-axis	90°	± 1.97	± 2.27	± 4.43

The self and mutual inductances of the MSBS coil system are calculated with the computer program EFFI. The inductance matrix is shown in Table III-5. The mutual inductances between coils are relatively small compared to self inductances.

A study of the operational effect on the maximum field, force and inductance are carried out. To illustrate the outcome of this study we take one of the drag coils as an example. The forces on this coil due to each of the four roll coils in the system are shown in Table III-6. A study of this table reveals that the maximum force in the x-direction on the drag coil from the roll coils alone is 43.64 MN. However, to produce this force, the current in two of the roll coils has to flow in an opposite direction to the current in the other two R coils. This is not realistic, because in all modes of operation, the current in each of the roll coils will be equal and in the same direction since the four roll coils operate in series. Thus these large forces cancel each other. A similar situation, but on a smaller scale, occurs for the drag, Z and Y coils. Every coaxial pair of these magnets will carry

Table III-5

Inductance Matrix in Milli Henries

Coil	Z-1	Z-2	Z-3	Z-4	Y-1	Y-2	Y-3	Y-4	X-1	X-2	R
Z-1	163										0
Z-2	6	163									0
Z-3	2	.8	163								0
Z-4	0.8	2	6	163							0
Y-1	+3.6	+0.7	-3.6	-0.7	163						0
Y-2	+0.7	+3.6	-0.7	-3.6	6	163					0
Y-3	-3.6	-0.7	+3.6	+0.7	2	0.8	163				0
Y-4	-0.7	-3.6	+0.7	+3.6	0.8	2	6	163			0
X-1	+30	+30	-30	-30	+30	+30	-30	-30	1824		0
X-2	-30	-30	+30	+30	-30	-30	+30	+30	62	1824	0
R	0	0	0	0	0	0	0	0	0	0	1907
	171.8	171.8	171.8	171.8	171.8	171.8	171.8	171.8	1886	1886	1907

almost the same current in the same direction during operation. It is desirable to connect each pair of these coils in series. However, this puts some restriction on the control requirements of these coils. Two possible solutions are considered. The first one is to separate the control function of the coil from the magnetic field requirements by adding an extra separate winding to each coil to perform the control function. In this case each pair of coils is connected in series with the control windings separate. The other solution, the one we adopt, is to design the control system in such a way to make it impossible to pass large currents in the magnets in a non-operational combination. This does not limit the usage of the system in any way but it makes the structural, power and material requirements more economical.

Table III-6

Forces and Torques on the Drag Coil due to the Roll Coils

Coil	F _x MN	F _y MN	F _z MN	T _y MN.m	T _z MN.m
R-1	10.91	2.00	-2.00	12.16	-12.16
R-2	-10.91	2.00	2.00	-12.16	-12.16
R-3	10.91	-2.00	2.00	-12.16	12.16
R-4	-10.91	-2.00	-2.00	12.16	12.16

III.3.2. Model Core Solenoid

The present model core solenoid has a pole strength increase of 18.7% from 3.75×10^4 to 4.45×10^4 Am due to the holmium winding cylinder. This is accomplished within the same size 70 cm long and 11.5 cm OD epoxy potted solenoid. The volume of contained liquid

helium is less due to the holmium volume. The best features of the previous configuration and operation in the persistent mode with 10A composite NbTi wire are retained. Coil parameters are listed in Table III-7.

Table III-7
Model Coil Parameters

Length (cm).....	70.0
Winding OD (cm).....	11.5
Winding ID (cm).....	8.26
Holmium mandrel OD (cm).....	8.26
Holmium mandrel ID (cm).....	6.14
Winding current density (A/m ²).....	3. x 10 ⁸
Operating current (A).....	10.
Peak winding field (T).....	6.1
Holmium magnetization (T).....	3.7
Number of turns.....	3.3978 x 10 ⁴
Conductor length (m)	1.055 x 10 ⁵
Conductor diameter (cm).....	0.02
Ac losses at full load (W).....	0.046

Design of the cryostat for the model core solenoid is nearly identical to the first concept. Supports are strengthened to cope with additional weight of the holmium core, the vent line is re-located for easier assembly, and volume displaced by holmium reduces helium capacity from 3.15 to 1.8 liters. For the loss rate of 0.16 l/h, the idling time for the helium level to fall from 90% to 50% is 4.5 hours. Sustained idle should be possible by refilling with helium on an eight-hour cycle. Holding time from 90% to 20% of capacity with a full load 10 Hz AC loss

of 0.046 W is approximately 5.6 hours. Although not shown in Fig. III.1, current thinking is to supply a battery powered radio "beeper" which would sound when the cryostat liquid helium level falls to the 20 or 25% full point. This would permit orderly shutdown of the wind tunnel for refilling the cryostat without immediate risk of running out of helium.

The concept cryostat design shown in Fig. III.1 illustrates major construction details. The inner helium/magnet container consists of a 117.5 OD X 0.254 mm wall outer stainless steel cylinder, 3.18 mm thick end plates and 57.15 OD x 1.59 mm wall inset tubes which double as cryostat support members and as magnet mounting cores. A prospective change is to add a perforated length of 57.15 tube to the center section to strengthen the inner container laterally and longitudinally.

Support of the inner shell starts with cantilever 50.8 mm OD G-11 epoxy-fiberglass tubes epoxied to internal end plates. Thicknesses of the two tubes are 1.27 and 1.79 mm front and rear to reflect their 70 and 95 mm moment arms. Exterior ends of the G-11 tubes are epoxied to support plates having a single pin at the front end and machined boss at the rear. The next support stage is from the pin/boss to intermediate stainless steel plates by means of epoxy impregnated S-glass fiber roving. Support is continued to the warm end plates by another set of three glass fiber filaments at each end. The intermediate stainless steel plates are attached to the copper vapor cooled shield both to support it and provide a heat intercept. Axial support of the inner shell assembly is provided by concentric G-11 tubes attached as shown. Removal of a former interference permits lengthening these tubes 25 mm with a heat leak reduction of about 24%.

Utilization of helium vent gas refrigeration is vital to thermal performance of the cryostat. This is accomplished by thermally shorting the vent line to the OFHC copper shield at both ends of the cryostat with copper wire or tabs. The front short is made just before the vent line turns toward the rear and the back short is made just as the vent tube emerges from the inner shell. To promote good heat exchange and reduce the possibility of convection currents or thermo-acoustic oscillation, the straight length of vent line will include a piece of thin, twisted stainless steel strip which will make helium vapor swirl as it exits the cryostat.

The outer shell is comprised of 3.18 mm thick end plates welded to a 126.2 OD x 0.711 mm thick stainless steel cylinder. The cylinder is designed for external pressure and will withstand careful handling. However, for wind tunnel loads the cryostat must either fit tightly into a mating cylinder or be supported from the ends which are structural hard points. Appropriate brackets or trunnions can be added to each end to facilitate mounting.

Thermal design of the cryostat is dependent on the low heat leak support system and low emissivity radiation surfaces. Low support heat leak is achieved by using a combination of G-11 fiberglass-epoxy tubes and high strength uni-directional S-glass or Kevlar filaments. Low emissivity surfaces result from use of OFHC copper, specially coated to resist oxidation, for the shield and by covering all exposed interior stainless steel surfaces with a Minnesota Mining and Manufacturing Co. (3M) aluminum tape. 3M tape has an emissivity on the order of 0.025 at room temperature and 0.01 at 4.2 K, which improve over stainless steel by about a factor of three. Emissivity of carefully prepared OFHC

copper at 70 K is between 0.015 and 0.02. With these values, radiation heat leak to the inner shell is only 2.44 mW compared to the support value of 6.71 mW. Shield heat leak is 1.28 W by radiation and 0.35 W due to supports. Vent gas refrigeration potential at 70 K is about 1.67 W.

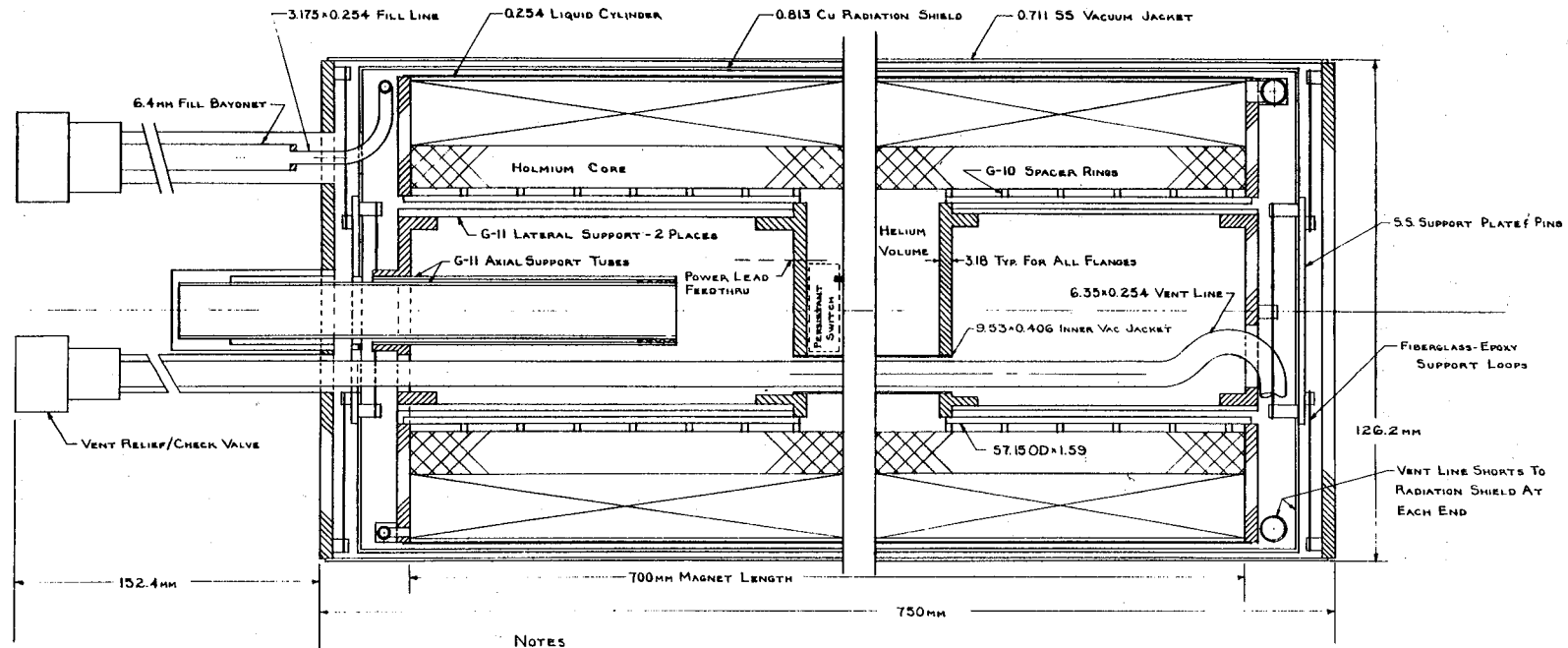
III.3.3. X, Y, Z and R Coils

The specifications for the X, Y, Z and R coils are listed in Tables III-8, III-9 and III-10. Note that most of the energy is stored in the X coils where it is contained by internal structure bifilar S.S. strip.

Table III-8

X Drag Coil Parameters

Number of coils.....	2.0
Operating current (kA).....	11.0
Winding current density (kA/cm ²).....	1.558
O.D. (m).....	5.514
I.D. (m).....	4.514
Height (m).....	0.7
Number of turns.....	496
Inductance (H).....	1.8
Energy stored/coil (MJ).....	108
Ampere-meters (MAm).....	85.9
Bifilar S.S. strip width (cm).....	0.42
Voltage for 10 Hz (V).....	830
AC losses/coil at ± 0.1% I at 10 Hz (W).....	96.0



- NOTES
1. COVER ALL INTERNAL SS SURFACES WITH 3M AL TAPE TO REDUCE EMISSIVITIES
 2. MATERIAL IS 304 SS EXCEPT AS NOTED
 3. USE G-11 BUMPERS (NOT SHOWN) FOR AXIAL SUPPORT OF SHIELD
 4. HELIUM VOLUME - 1.8 LITERS TOTAL
 5. STATIC HOLD TIME FROM 90% TO 90% ~ 4.5 HOURS

Figure III.1. Core Magnet Cryostat.

Table III-9

Z or Y Coil Parameters

Number of coils.....	4
Operating current (kA).....	11.0
Winding current density (kA/cm ²).....	2.065
O.D. (m).....	2.306
I.D. (m).....	1.289
Height (m).....	0.3
Number of turns.....	286
Inductance (H).....	0.156
Energy stored/coil (MJ).....	9.47
Ampere meters (MAM).....	17.79
Bifilar S.S. strip thickness (cm).....	0.224
Voltage for 10 Hz operation (V).....	76
AC losses/coil at 0.1% I at 10 Hz (W).....	18.8

Table III-10

Roll Coil Specifications

Saddle coils in series (number of coils).....	4
Operating current (kA).....	11
Winding current density (kA/cm ²).....	1.765
Turns/saddle coil.....	240
Total turns (4 coils).....	960
Inductance (4 series coils) (H).....	1.91
Energy stored (MJ) (4 coils).....	116
Ampere-meters (MAM) (4 coils).....	154
Bifilar stainless steel thickness (cm).....	0.19
Voltage for 10 Hz operation (V).....	840
Ac losses at 0.1% dynamic force at 10 Hz (W).....	180

The coil weights are divided between the interleaved stainless steel strip, 0.42 cm to 0.19 cm thick, and the conductor which includes a 0.1 cm strip of internal steel. The weights are listed in Table III-11.

Table III-11

Coil Weights, kg

Coils	R	X	Y	Z
Conductor	15,980	8,870	1,675	1,675
S.S. trip (width cm)	7,344 (0.19)	9,216 (0.42)	1,000 (0.22)	1,000 (0.22)
Total	23,324	18,080	2,675	2,675
No. Coils	1*	2	4	4
Total weight (kg)	23,324	36,172	10,700	10,700
Sum		80,896		

*Four series saddle coils treated as one coil.

The AC losses in the coils and stainless steel structural interleaved strip at 10 Hz for full and quarter load are listed in Table III-12. Hysteresis for the 6.7 μm filaments of NbTi is the major loss item. At quarter load hysteresis is only about half the value at full load while the eddy current losses are reduced to 1/16.

The eddy current losses into the liquid helium from 10 Hz AC induced currents in nearby cold S.S. structures (Table III-13) are small compared to the losses in the 1984 design because the structure is mostly non-metallic with little stainless steel for the X coils.

TABLE III-12

Coil AC Losses at 10 Hz

Coil	R	X	Y	Z	Sum
Hysteresis	138	76	15.4	15.4	
Conductor	27	15	3.1	3.1	
S.S. strips	15	5	0.3	0.3	
Total	180	96	18.8	18.8	
No. coils	1	2	4	4	
Total, full load	180	192	75.2	75.2	522 W
Total, quarter load	71.6	78.5	31.65	31.65	213.4

Table III-13

Eddy Current Losses in Structure and Helium Vessel

Power loss at full load	200 W
Power loss at 1/4 load	50 W

IV. SYSTEM ANALYSIS

IV.1. Parametric Study

Ampere-meters (IS) of conductor and stored energy (E) in the X, Y, Z and R coils are the two major cost-related parameters to be optimized. The most interesting variables are coil self fields and coil current densities. MSBS coils are required to produce small fields, 0.1 to 0.17 tesla, at the airplane model pole tips instead of the more standard requirement of a quality high field in the bore of a solenoid. As an example we consider one of the Z (Lift) coils. Tables IV-1, IV-2, IV-3, and IV-4 list coil height (H), inner radius (R_1), outer radius (R_2), ampere-meters (IS), and energy stored (E) as functions of the gross current density (J) and maximum field in the winding (B_m). As seen, the higher the design field, the smaller the inner radius. Other parameters do not change appreciably as the maximum field, B_m , increases above 4 tesla. Fields lower than 4 tesla tend to increase the coil outer radius which is limited by coil interference. Figures IV.1 and IV.2 are plots of IS and E vs. J from the above tables. The conclusion is that there are broad minima in IS and E which allow wide latitude in selecting an optimized J. The selections here are 4.5 T and 1500 to 2500 A/cm² for the MSBS design.

IV.2. Conductors

The objective of this section is to evaluate and select conductors for different methods of cooling. The three choices are: 1) Conductors cooled by pool boiling in 4.2 K helium baths. 2) Conductors cooled by pressurized superfluid helium in 1.8 K baths. 3) Conductors cooled by

Table IV-1

Z Coil Dimensions, Ampere-meters and Energy Stored
as Functions of Maximum Winding Field
and Gross Current Density

$$J = 1500 \text{ A/cm}^2$$

B_m (T)	H (m)	R_1 (m)	R_2 (m)	IS (MAm)	E (MJ)
3	0.20	0.56	1.46	17.06	8.77
	0.25	0.70	1.40	17.31	9.49
	0.30	0.84	1.39	17.30	9.52
4	0.20	0.24	1.41	18.15	7.89
	0.25	0.36	1.28	17.82	8.81
	0.30	0.45	1.21	17.89	9.53
5	0.20	0.10	1.41	18.55	7.07
	0.25	0.17	1.27	18.72	8.18
	0.30	0.25	1.18	18.73	9.08
6	0.20	0.02	1.41	18.64	7.00
	0.25	0.07	1.26	18.74	7.34
	0.30	0.12	1.17	19.29	8.53

forced flow supercritical helium at temperatures above 5.2 K. The amounts of copper and superconductor, the AC and helium pumping losses, and the reliabilities are compared for the three different cooling schemes.

IV.2.1. Conductor for pool boiling. The cabled conductor shown in Fig. IV.3 is the well qualified ANL 11 kA pulsed conductor [9] for pool cooling. The cables are fabricated by twisting 24 basic cables around an insulated stainless steel strip with a twist pitch of 22.5 cm. The basic cable is three seven-strand conductors (triplex cable) twisted with a 2.2 cm pitch. The seven-strand triplex cable is six OFHC copper

Table IV-2

Z Coil Dimensions, Amper-meters and Energy Stored
as Functions of Maximum Winding Field
and Gross Current Density

$$J = 2500 \text{ A/cm}^2$$

B_m (T)	H (m)	R_1 (m)	R_2 (m)	IS (MAm)	E (MJ)
3	0.25	1.25	1.57	17.48	10.18
4	0.20	0.62	1.19	16.25	10.14
	0.25	0.73	1.18	16.85	10.77
	0.30	0.79	1.16	16.78	10.46
5	0.20	0.39	1.12	17.22	10.42
	0.25	0.49	1.07	17.90	11.77
	0.30	0.55	1.03	17.91	11.93
6	0.20	0.23	1.08	17.56	9.47
	0.25	0.33	1.02	18.28	11.36
	0.30	0.39	0.98	19.14	12.81
7	0.20	0.13	1.09	18.26	9.09
	0.25	0.21	1.01	19.20	11.14
	0.30	0.28	0.96	19.66	12.55

wires twisted around a superconducting center conductor and all soldered with Staybrite. Since the requirements of low AC losses and cryostability conflict with each other, the basic principle chosen is to achieve cryostability within the basic cable. To restrict AC coupling among the 24 triplex cables in the final cable, only limited current sharing among the triplex is allowed by coating a thin insulating film around the seven-strand conductors. Each superconducting strand has a diameter of 0.051 cm and contains 2041 filaments of 6.7 μm dia with a twist pitch of 1.27 cm. The copper-to-superconductor ratio for each superconducting strand is 1.8.

Table IV-3

Z Coil Dimensions, Ampere-meters and Energy Stored
as Functions of Maximum Winding Field
and Gross Current Density

$$J = 3500 \text{ A/cm}^2$$

B_m (T)	H (m)	R_1 (m)	R_2 (m)	IS (MAm)	E (MJ)
4	0.20	0.93	1.26	15.88	10.29
	0.25	0.98	1.25	16.31	10.34
	0.30	0.97	1.20	16.35	10.13
5	0.20	0.62	1.06	16.33	11.48
	0.25	0.69	1.04	16.70	11.74
	0.30	0.73	1.03	17.20	11.99
6	0.20	0.43	0.98	17.25	12.29
	0.25	0.52	0.96	17.65	13.07
	0.30	0.57	0.94	18.23	13.66
7	0.20	0.31	0.97	18.49	12.86
	0.25	0.38	0.91	18.74	19.00
	0.30	0.43	0.87	18.86	14.36

Table IV-4

Z Coil Dimensions, Ampere-meters and Energy Stored
as Functions of Maximum Winding Field
and Gross Current Density

$$J = 4500 \text{ A/cm}^2$$

B_m (T)	H (m)	R_1 (m)	R_2 (m)	IS (MAm)	E (MJ)
4	0.25	1.16	1.34	16.27	10.00
	0.40	1.16	1.32	16.63	10.01
5	0.20	0.79	1.08	15.50	10.87
	0.25	0.83	1.07	16.54	11.71
	0.30	0.85	1.06	16.68	11.91
6	0.20	0.57	0.95	16.44	12.61
	0.25	0.63	0.94	16.86	11.87
	0.30	0.67	0.92	17.42	13.18
7	0.20	0.44	0.90	17.48	13.91
	0.25	0.51	0.88	17.99	14.64
	0.30	0.55	0.86	18.58	15.17

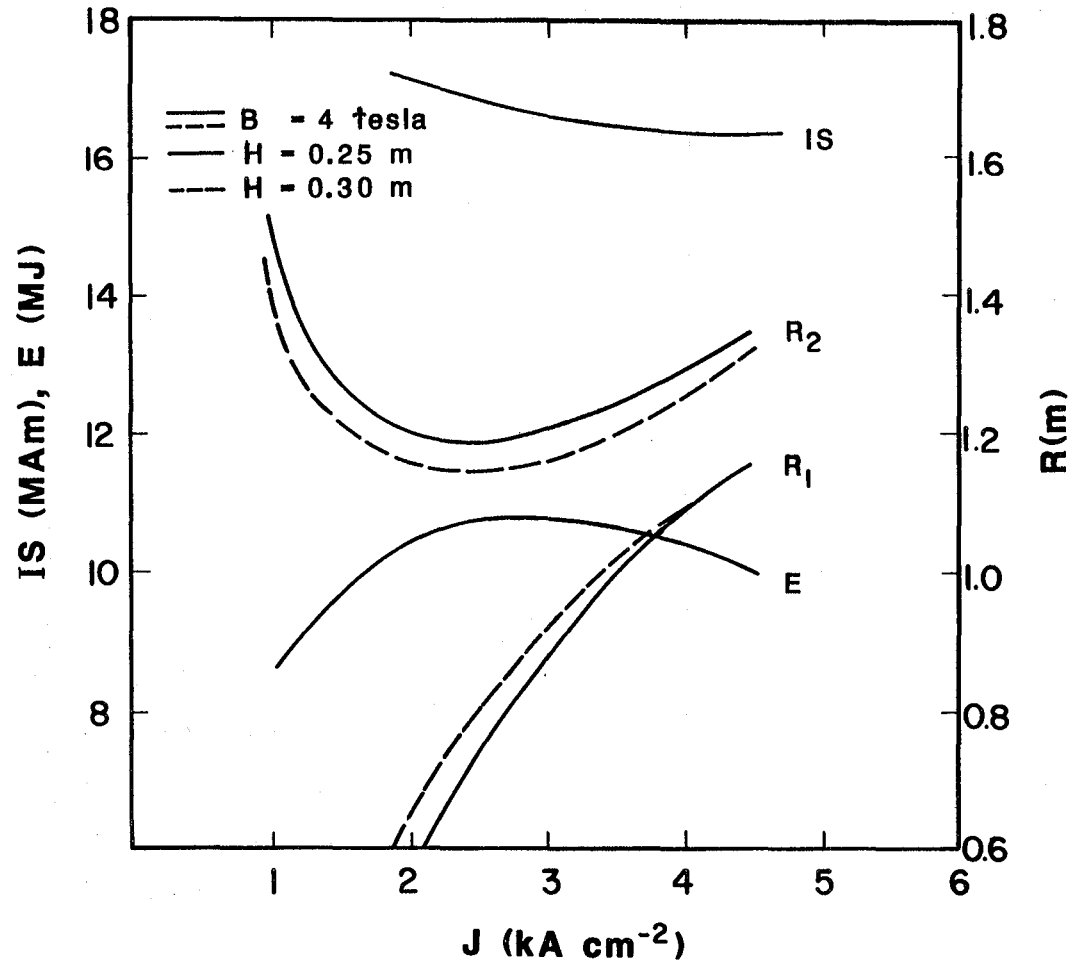


Figure IV.1. Z or Y coil parameters vs. gross current density J . IS is ampere-meters, E is energy stored, R_1 is inner radius, and R_2 is outer radius.

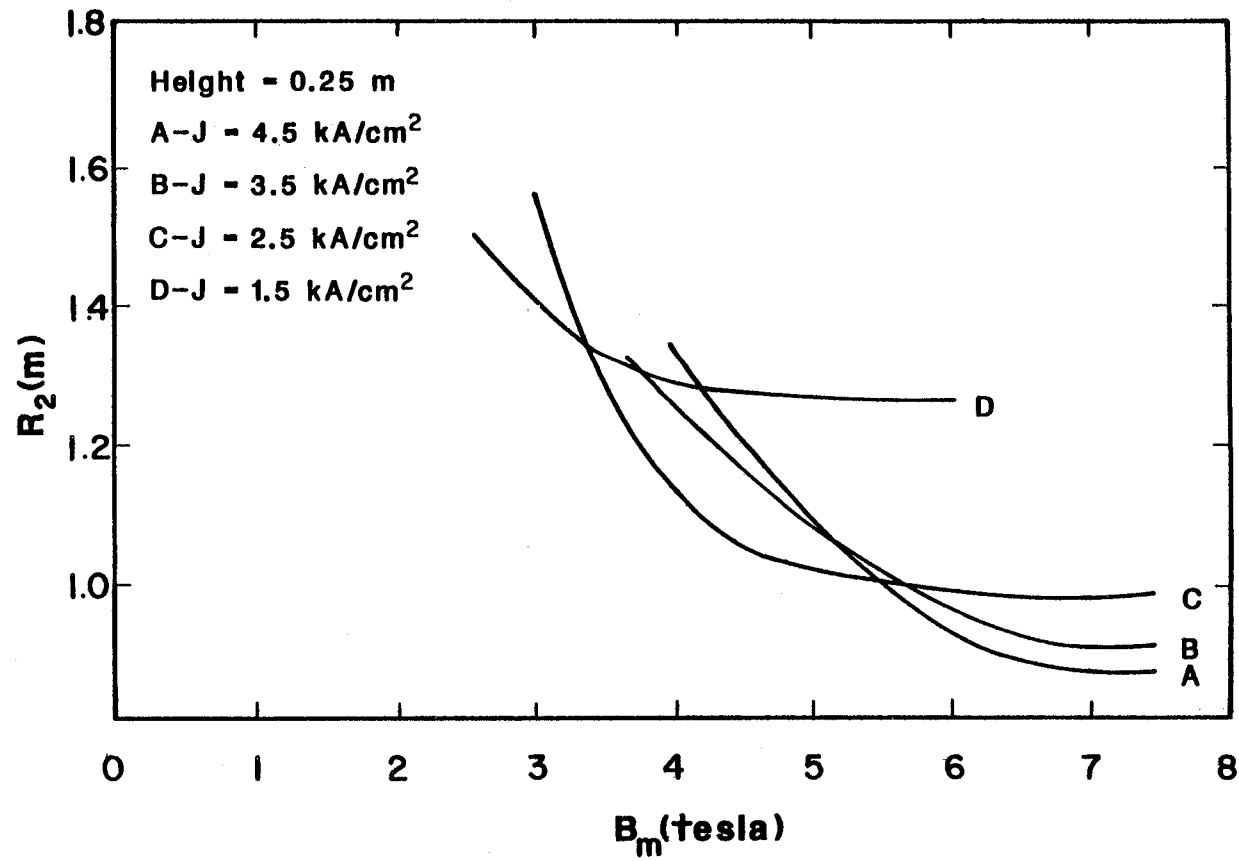


Figure IV.2. Z or Y coil outer radius as function of maximum self field plotted for different gross current densities.

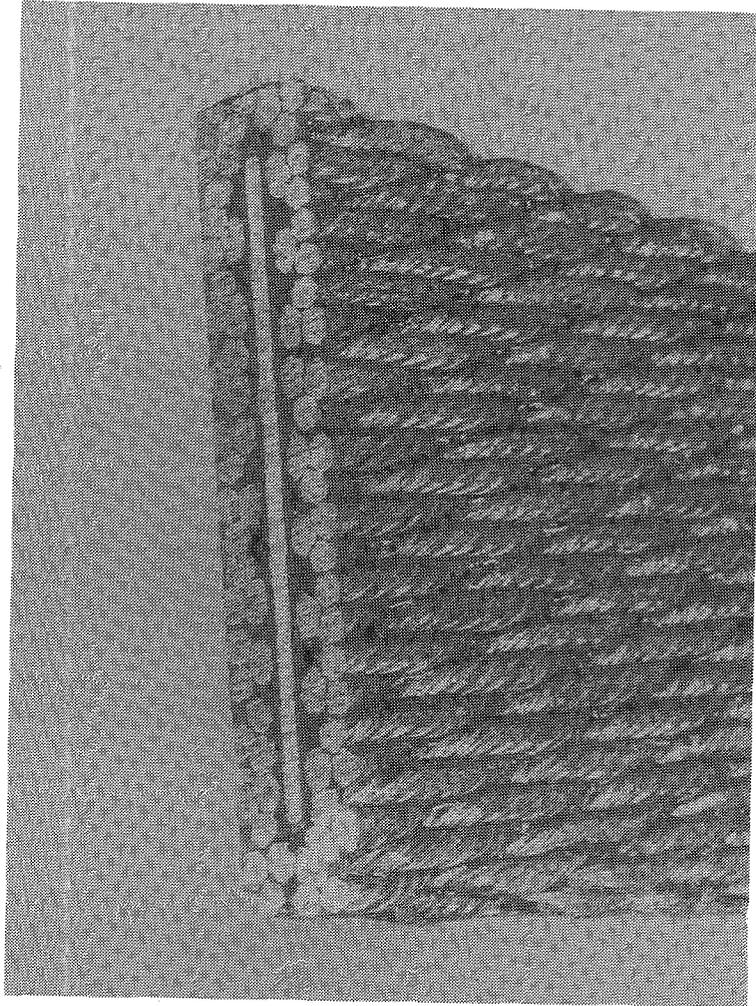


Figure IV.3. Cryostable 11 kA AC cable.

Table IV-5

Characteristics of the ANL Cable Conductor (9)

No. of strands.....	504
Strand diameter (cm).....	0.051
No. of filaments per strand.....	2041
Filament diameter (μm).....	6.7
NbTi area (cm^2).....	0.0518
Copper area (cm^2).....	0.9636

The final cable is compressed during the cabling by heavy rolls from four sides. This minimizes mechanical perturbations of the basic conductors during pulsing. The compression does not damage the insulation between the 0.1 cm central stainless steel strip and the 24 triplex cables. However, owing to the deformation of the soft solder in the seven-strand conductor, about 5% degradation of the recovery current occurs. The MSBS magnet design with interleaved 0.19 cm to 0.42 cm thick stainless strips between turns relieves the necessity to square up a winding with accurate cable compression since the strips, not the cable, govern the winding. The finished cable has a width of 3.78 cm and a thickness of 0.74 cm.

IV.2.1.1. 4.2 K pool cooling. At 4.2 K the ANL conductor is designed to carry 11 kA at 4.5 tesla with a surface recovery heat flux equal to 0.35 watt/cm². Operation at higher fields will require adding NbTi to the conductor. Tables IV-5 and IV-6 list the Cu and NbTi per ampere-meter, and the 10 Hz losses for $\pm 0.1\%$ field variation.

IV.2.1.2. 1.8 K pool cooling. At 1.8 K the critical current density of NbTi is 60% more than at 4.2 K or 17.6 kA for the ANL conductor at 4.5 tesla. The design recovery heat flux is 0.9 watt/cm² which is typical for superfluid helium pool cooling at 1 atmosphere. If the same conductor is used at 1.8 K then the same stability criteria are still met since I^2R (non-superconducting at 1.8 K) increases by a factor of 2.56 while available cooling increases by a factor of 2.57. The operational characteristics of the ANL cable used in 4.2 K-one atmosphere pool cooling and in 1.8 K-one atmosphere pool cooling are compared in Table IV-6.

Table IV-6

ANL Cable Conductor for 4.2K and 1.8 K Operation

	4.2 K	1.8 K
Operating current (kA)	11	17.6
Maximum field (T)	4.5	4.5
Cryostable recovery heat flux (W/cm ²)	0.35	0.9
Hysteresis loss (J/cycle/m*) ($\times 10^{-4}$)	9.5	9.5
Eddy current (J/cycle/m*) ($\times 10^{-4}$)	1.92	1.92
Conductor length (relative)	1.6	1
Current density (A/cm ²)	1500	2400
Refrigeration power (relative)	1	3

*Losses for $\pm 0.1\%$ I at 10Hz.

In conclusion, the performance for 4.2 K and 1.8 K cooling seem about the same for 4.5 tesla fields. The comparative choice is to select 4.2 K cooling today. However, research on 1.8 cooling in cramped conditions such as in MSBS designs could lead to choosing 1.8 K pool cooling in the future. Less conductor and more compact coils for 1.8 K are both attractive.

IV.2.2. Forced Flow Cooling. The conductor chosen is a modified version of the J15 conductor (Fig. IV-4) developed at the Japan Atomic Energy Research Institute for Tokamak pulsed poloidal field coils [4]. The 15 kA conductor is designed to optimize stability and minimize hysteresis and eddy current losses. Table IV-7 lists major specifications of the J15 conductor. Pressure drops, friction factors and conductor stabilities were found for helium flow rates of 5 to 8 grams/sec. At 5 g/s, the flow work (pumping loss) is 7.512×10^{-2} W/m which is equivalent to 4.767 W/MAm. A total of 1500 watts of flow work

will be required for all 14 MSBS coils, which is substantial compared to other losses in the MSBS system. Other advantages and disadvantages of forced flow cooling are discussed in IV.3.

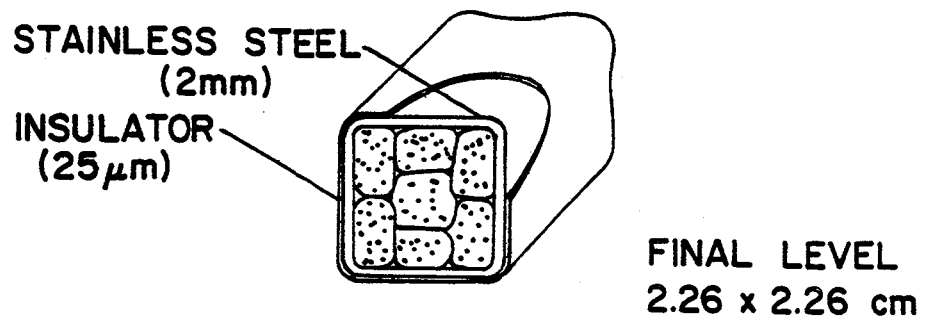


Fig IV.4. 15 kA Forced Flow Conductor.

Table IV-7

JF-15 Forced Flow Conductor [Ref. 7]

Current (kA at 4.5T).....	15.
Helium flow (g/s).....	5.
Square conduit side (mm).....	22.6
Internal conduit area (mm) ²	346.
Strand area (mm) ²	230.
Helium area (mm) ²	112.
Cooling length (m).....	32.
Number of strands.....	189.
Diameter of each strand (mm).....	1.18
Strand: (Nb-Ti/Cu/Cu-Ni).....	0.09/0.95/1
Nb-Ti filaments/strand.....	1560
Filament diameter (μm).....	6.7

IV.3. Cooling Methods

The characteristics, advantages and disadvantages of the three cooling schemes are summarized below.

IV.3.1. Pool cooling at 4.2 K. In this simple method of cooling, the stability criterion is that I^2R in a non-superconducting composite conductor should generate less than 0.3 W/cm^2 , the recovery heat flux for film boiling. Such stability is the best, most conservative stability of the three cooling systems. The current density is the lowest. The refrigeration power for heat loads at 4.2 K is about 300 W/W.

IV.3.2. Superfluid helium at 1.8 K. Very large heat transfer coefficients (up to 2 watts/cm²) are possible using HeII at 1.8 K. The advantages of using HeII cooling are not only in stability and filling factor for higher gross current density, but also in critical current density in NbTi, by virtue of reduced 1.8 K temperature. A major

disadvantage of this kind of cooling, especially for AC coils, is that refrigeration power of about 900 W/W is required to remove the low temperature heat load.

IV.3.3. Forced flow cooling. There are several advantages over pool boiling conductors: continuous electrical insulation eliminates the possibility of shorts between turns, simpler coil and cryostat construction, operation at temperatures higher than 4.2 K with Nb_3Sn , and higher gross current densities due to higher surface heat flux. However, there are disadvantages compared with pool boiling. First, stability is a short-term affair (ms) because of the small amount of helium in the system. Second, force cooled systems deposit heat in the conduit due to helium flow friction which is cooled by the flowing helium. Third, the amount of superconductor is high compared to pool boiling and much higher compared to HeII cooling. Accordingly, forced flow cooling is advantageous for low stability, high field, high current density magnets, such as fusion toroidal coils.

IV.3.4. Conclusions. Based on the characteristics, advantages and disadvantages of the three methods of cooling, the following is concluded:

- * Pool cooling at 4.2 K-one atmosphere is the conservative reliable choice.
- * Superfluid cooling at 1.8 K adds about 3.5% to the overall system cost and is possibly more stable but is less tested.
- * Forced flow cooling provides less stable and higher current densities which are not needed for MSBS. The main disadvantage is the large pumping losses, 1500 W for MSBS magnets.

A rough analysis of relative costs of using each cooling system for the MSBS system is given in Table IV-8. As shown, there is no clearcut financial advantage for any of the three. However, 4.2 K pool boiling is the conservative choice.

Table IV-8

MSBS Cost Differences for 1.8 K HeII and Forced Flow Cooling
Compared to 4.2 K Cooling

	Forced Flow	1.8 K HeII
Cryostat	- 500,000	+ 325,000
Magnets	~ same	- 750,000
Liquefier	+ 1,250,000	+1,192,000
Other cryogenic systems	- 400,000	-
Total (\$)	+ 350,000	+ 767,000

IV.4. AC Losses and Control Requirements

IV.4.1. External Magnet Losses and Control Limits

Magnet AC losses arise from the rapid variation in magnet currents and the magnetic fields used to vary the forces at the pole tips and wings of the airplane model. The control requirement is $\pm \Delta I\% \leq \pm 0.1\% I_{\max}$ at $f = 10$ Hz. However, the 11 kA Argonne conductor in magnets can withstand $B < 11$ T/s without quenching. It is interesting to determine the control force and rate limits if magnet stability is the only criterion. For example, assume that $B < 6$ T/s is the limit.

Taking $\pm \Delta I\%$ sinusoidal variation in I at frequency f and B as the maximum field in the windings of one of the 14 external magnets we find that:

$$B = 0.02 \pi f \Delta I B$$

For $\dot{B} = 6 \text{ T/s}$ and $B = 6\text{T}$ the limiting relation is:

$$[\Delta I f]_{\max} = 16.$$

Maximum values of ΔI vs. f listed in Table IV-9 are those maximum values for which magnets will not quench.

Table IV-9

Maximum Control Variation of Current vs. Control Frequency

f (Hz)	10	25	50	100	160
$\pm \Delta I$ (%)	1.6	0.64	0.32	0.16	0.1

The magnets can tolerate a percentage current variation \times frequency product which is 16 times larger than the control requirement of $\pm 0.1\%$ I at 10 hz. However, there are two other limits for higher values of $\Delta I f$. The first limit is the eddy current loss in the system structure, which is proportional to $(\Delta I f)^2$. Structure losses dominate other losses if metallic structure is used. The use of a non-metallic composite structure eliminates most eddy current losses and allows higher control requirements without extensive helium use.

IV.4.2. Model Coil Losses and Control Limits

The second limit on $\Delta I f$ is the AC loss in the model coil turns and mandrel which determines boil-off rate and running time of the model coil. The AC loss in the turns is mostly hysteresis loss in the NbTi filaments. The second loss is the eddy current loss in the holmium

mandrel. $\Delta I f = 1$ for 10 Hz and 0.1% current variation. The hysteresis loss is 4.5×10^{-3} J/cycle (0.045 watt) and the eddy current loss in holmium is 0.6×10^{-4} W. In general for ΔI and f the power loss is

$$P = 0.045 [\Delta I f] + 0.5 \times 10^{-4} [\Delta I f]^2 .$$

For reasonable values of $\Delta I f$, the second term in the above equation can be neglected.

Heat leak losses in the model coil are:

Radiation.....	9 J/h
Lateral supports.....	145
Vent line.....	10
Axial support.....	127
Fill line.....	62
Miscellaneous.....	47
Total	<u>400 J/h</u> (0.111 W)

Accordingly, the total power loss during full operation is

$$P_t = 0.111 + 0.045 \Delta I f .$$

Power loss and helium loss rate vs. $\Delta I f$ are listed in Table IV-10.

Table IV-10

Model Coil Losses vs. $\Delta I f$

$\Delta I f$	1	5	10	15
P_t (W)	0.156	0.336	0.561	0.786
Loss rate (l/h)	0.223	0.484	0.808	1.132

Based on the loss rates for the model solenoid and the use of composite structure for external coils, control requirements can be increased above the present value of $\Delta I f = 1$ to $\Delta I f = 3$ without adding significant AC losses to either the model coil or the external coils. The use of smaller filament size in the model coil would reduce the hysteresis loss and provide more chance for a higher control $\Delta I f$ factor if needed.

IV.5. Drag Coil Requirements

Are drag coils required? The answer is yes, at least one drag coil is required. Practically it is better to have two drag coils to minimize ampere-meters. The proof is as follows:

Case I: Consider the use of the 4 Z coils to produce the drag force, lift force and pitch moment. First specify F_x and F_z at both pole tips of the model coil which is 4 constraints. An extra constraint to be satisfied is $\nabla \times B = 0$ in the XZ plane, $\frac{\partial B_x}{\partial z} = \frac{\partial B_z}{\partial x}$.

Thus we have 5 constraints and 4 Z coils which means we need at least one drag coil.

Case II: Similar arguments can be applied for the use of the 4Z and 4Y coils to produce drag, lift, and side forces plus pitch and yaw moments. Now we have 6 forces to specify at model pole tips and three other constraints from $\nabla \times B = 0$, i.e., 9 constraints and 8 coils. Again one drag coil is needed. For symmetry two drag coils would be preferred.

V. STRUCTURAL AND THERMAL DESIGN

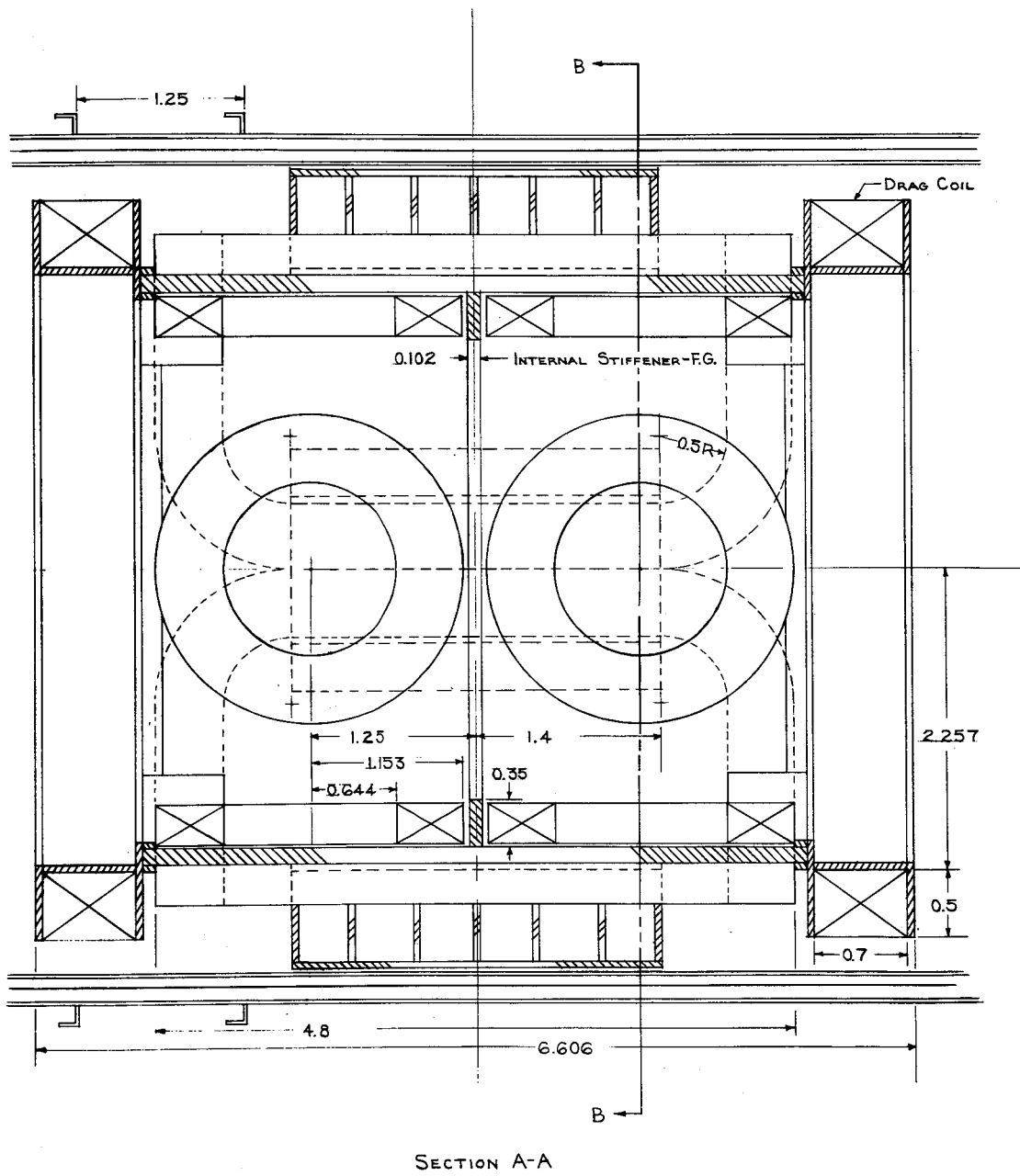
V.1. Structure Concepts

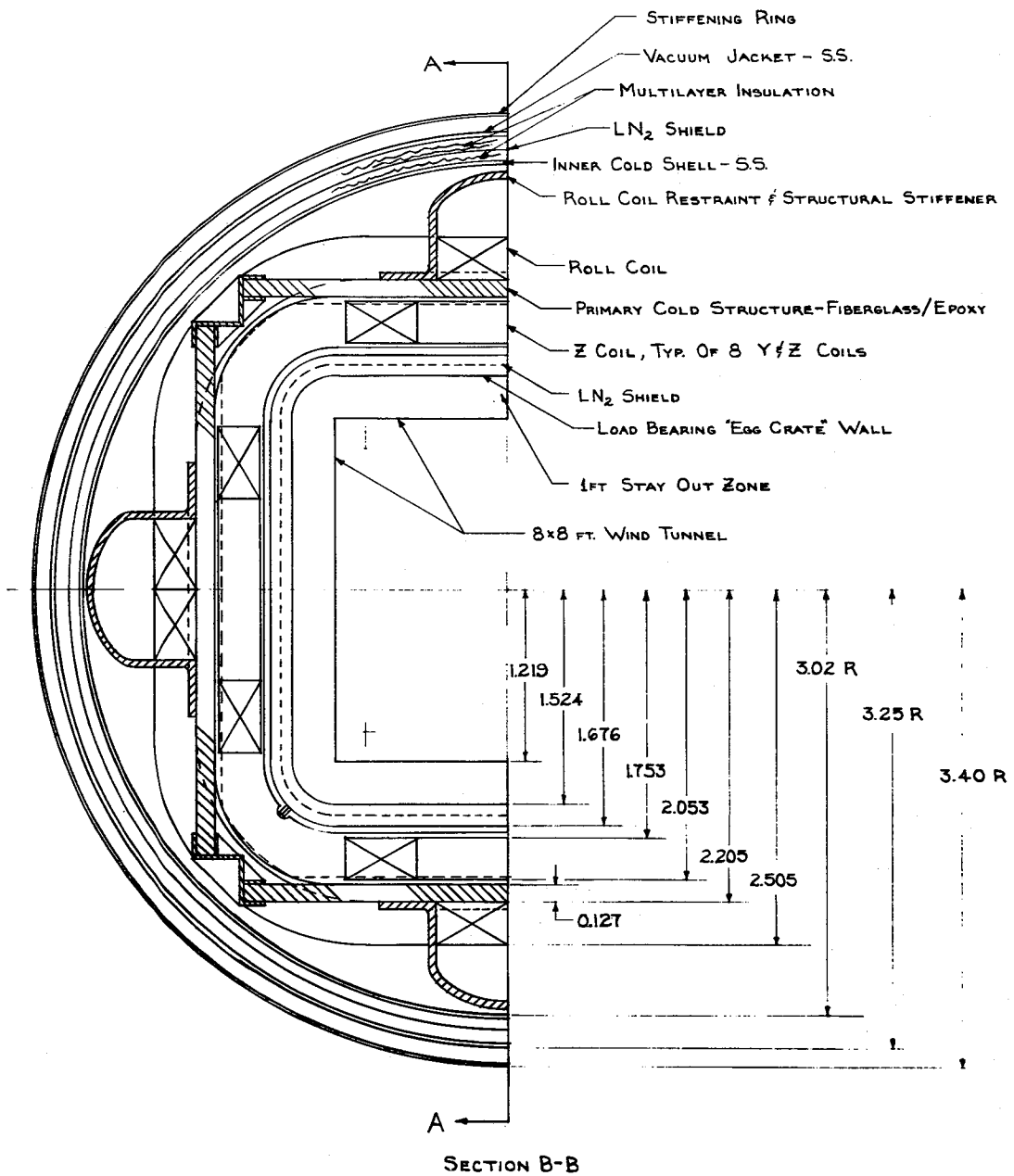
There are four structural design drivers:

1. Size and location of the magnets.
2. Magnet forces and torques.
3. Choice between individual or one common magnet cryostat.
4. Design and material selection to minimize eddy current losses.

In the 1984 design it was determined that there were significant structural and thermal advantages to having all of the magnets in a common cryostat. This arrangement allowed the magnets to be as close as possible to the wind tunnel and to each other and eliminated the thermally inefficient transfer of forces from cold to warm and back to cold structure. It was also learned that metallic structure eddy current losses had the major impact on the size and cost of the cryogenic system.

The new structural design retains the best features of the 1984 design and incorporates several improvements. Aside from the continuing use of a common liquid helium cryostat, the principal retained structural feature is the low heat leak load-bearing "egg-crate" thermal-vacuum enclosure immediately around the wind tunnel. This gets the magnet array as close as possible to the tunnel with only a 2 mm thickness stainless steel sheet between the magnets and the model coil. This thin sheet is essentially transparent to the 10 Hz control field penetration.





Dimensions are in meters.

Figure V.2. Cryostat Transverse Section

The principal new structural design feature is the separation of magnet structure from helium containment. As shown in Figs. V.1 and V.2, all of the control magnets are attached to a freestanding structural assembly which is not fastened to the cryostat walls. Further, except for longitudinal corners and end assemblies, the structure is epoxy-fiberglass which produces no eddy current heating. Both the inner and outer cold walls of the cryostat have longitudinal electrical breaks and the combination end plate/drag coil containment assemblies each have radial breaks. These features reduce full load structural eddy current losses from 1560 to 200 W.

Compared to the 1984 design, the overall size and weight of the MSBS assembly is reduced, the length is increased by 0.2 m because of the re-positioned drag coils and the diameter is smaller. The vacuum jacket diameter over the drag coils is now 6.5 m. The weight of the cryostat assembly and magnet attachments is 125,310 kg, a reduction of 35.2%. Costs are reduced by a somewhat greater percentage despite the higher base cost of fiberglass-epoxy compared to stainless steel, because field fabrication and assembly labor are less.

Fewer drawings were prepared for the current work because of its similarity to the 1984 MMI concept design and the more specific task focus. Thus, Figs. V.1 and V.2 are the principal representations of the new design. These sectional views do not include overall longitudinal dimensions, and support legs are not shown; but other mechanical details and dimensions are reasonably complete. These two figures are supplemented by several detail drawings. Electrical break concept designs for the end assemblies, cylindrical cold shell and egg crate cold wall are shown in Figs. V.3, V.4 and V.5, respectively. A view of the stainless

steel end plate assembly is given in Fig. V.6 and a section of the roll coil restraint tunnel is shown in Fig. V.7. Discussion of details illustrated in these figures is included in following sections.

V.2. Materials

Materials for the cryostat are selected for low temperature compatibility, optimum properties and cost. The material list with principal applications and properties follows:

304 S.S.--Used for inner and outer walls of the cryostat and for external stiffening rings. Design stress = 129.6 MN/m^2 .

304N--Higher strength version of 304 stainless steel used for the end plate assemblies and corner brackets. Design stress = 137.9 MN/m^2 .

Nitronic 40 (UNS 521900)--Used for high strength cryogenic bolts and pins. Room temperature ASME stress = 155.13 MN/m^2 .

Invar--Invar is useful for washers because of its low shrinkage in cooling to helium temperature. Although working stress is not a big factor, the ASME allowable for Invar is 115.8 MN/m^2 .

G-10 and G-11 Fiberglass-Epoxy--Main structural slabs and the roll coil tunnels will be made of epoxy-fiberglass which should have properties equal to G-10. Weight-bearing portion of the egg crate assembly will be made of commercial G-11 because of its superior vacuum properties. Maximum design stress for these composites is 137.9 MN/m^2 .

Dimensions are in millimeters.

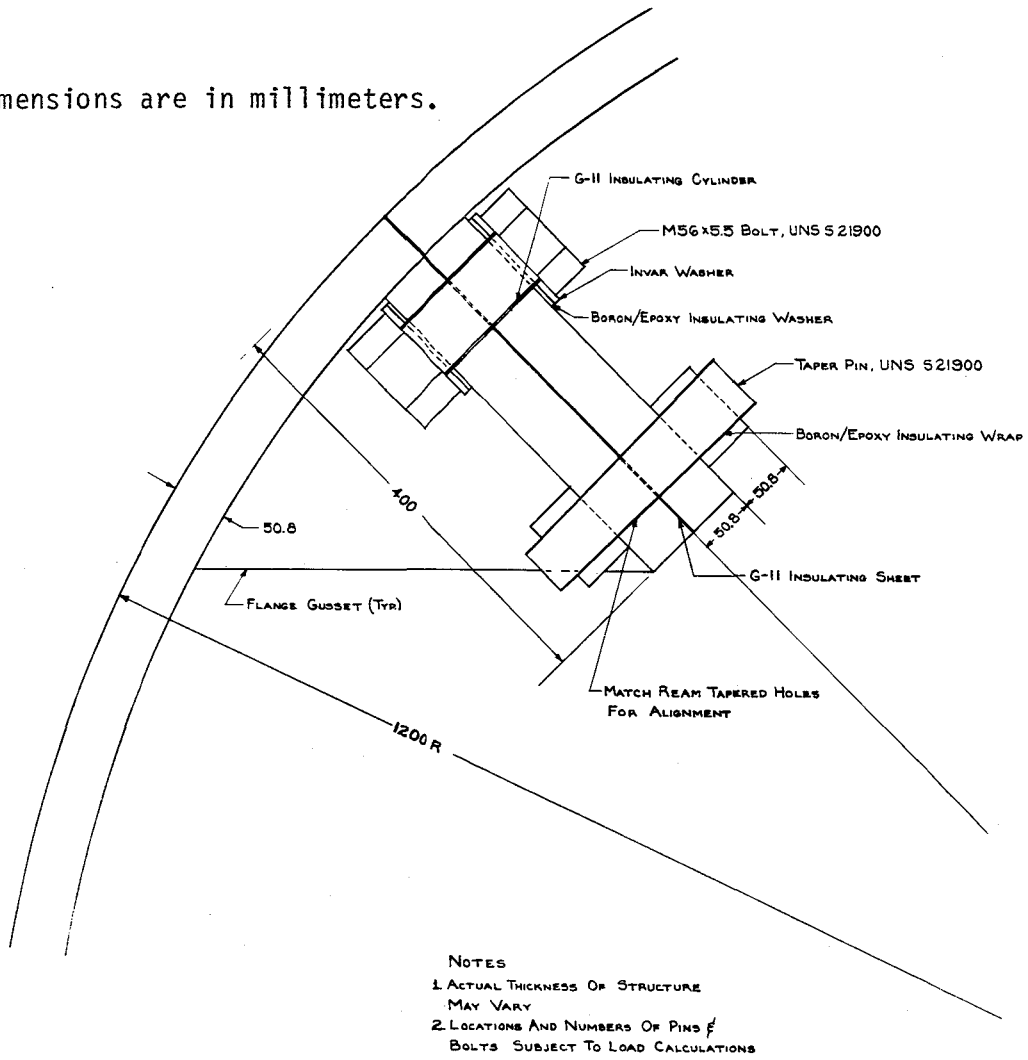


Figure V.3. Structural Electrical Break

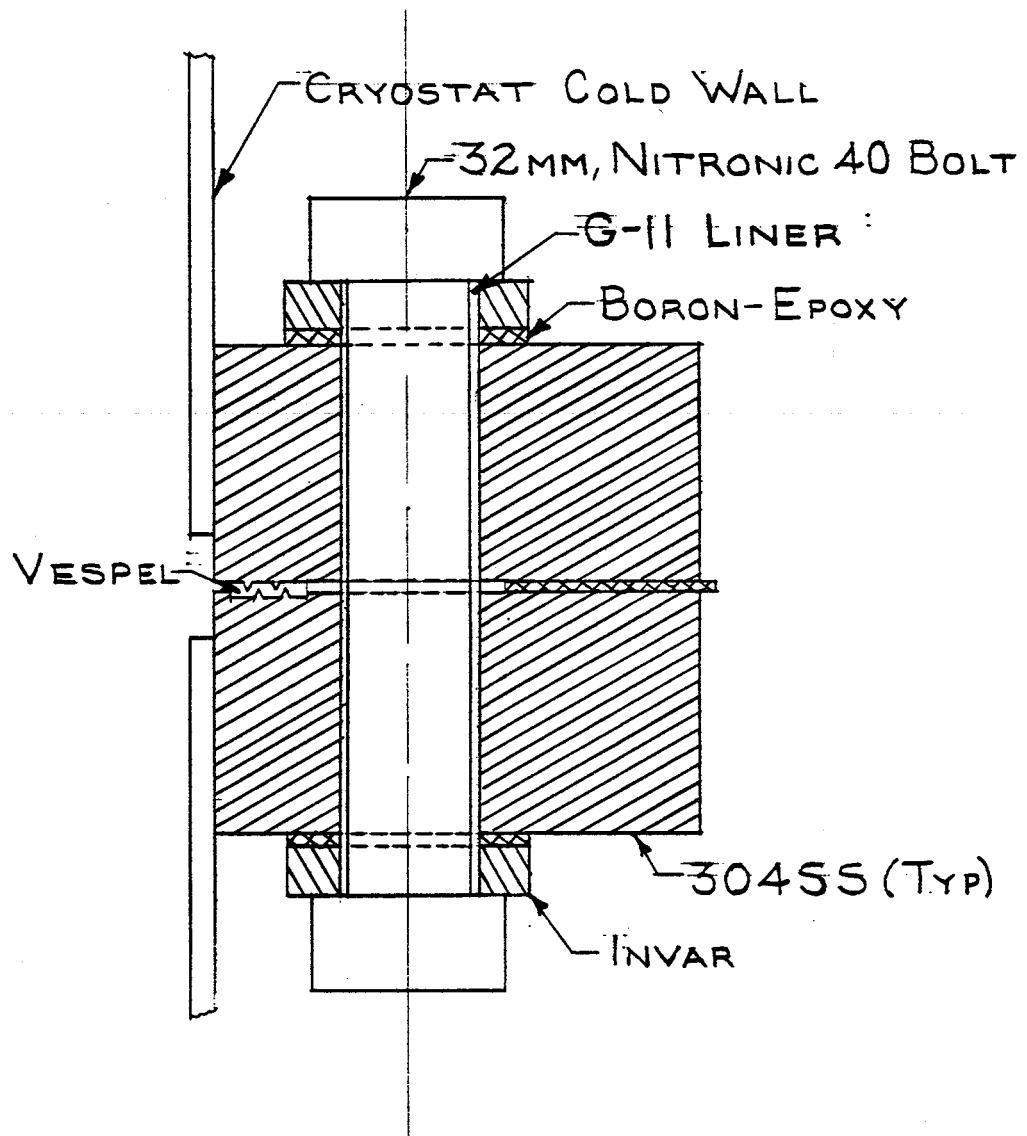


Figure V.4. Cold Shell Electrical Break

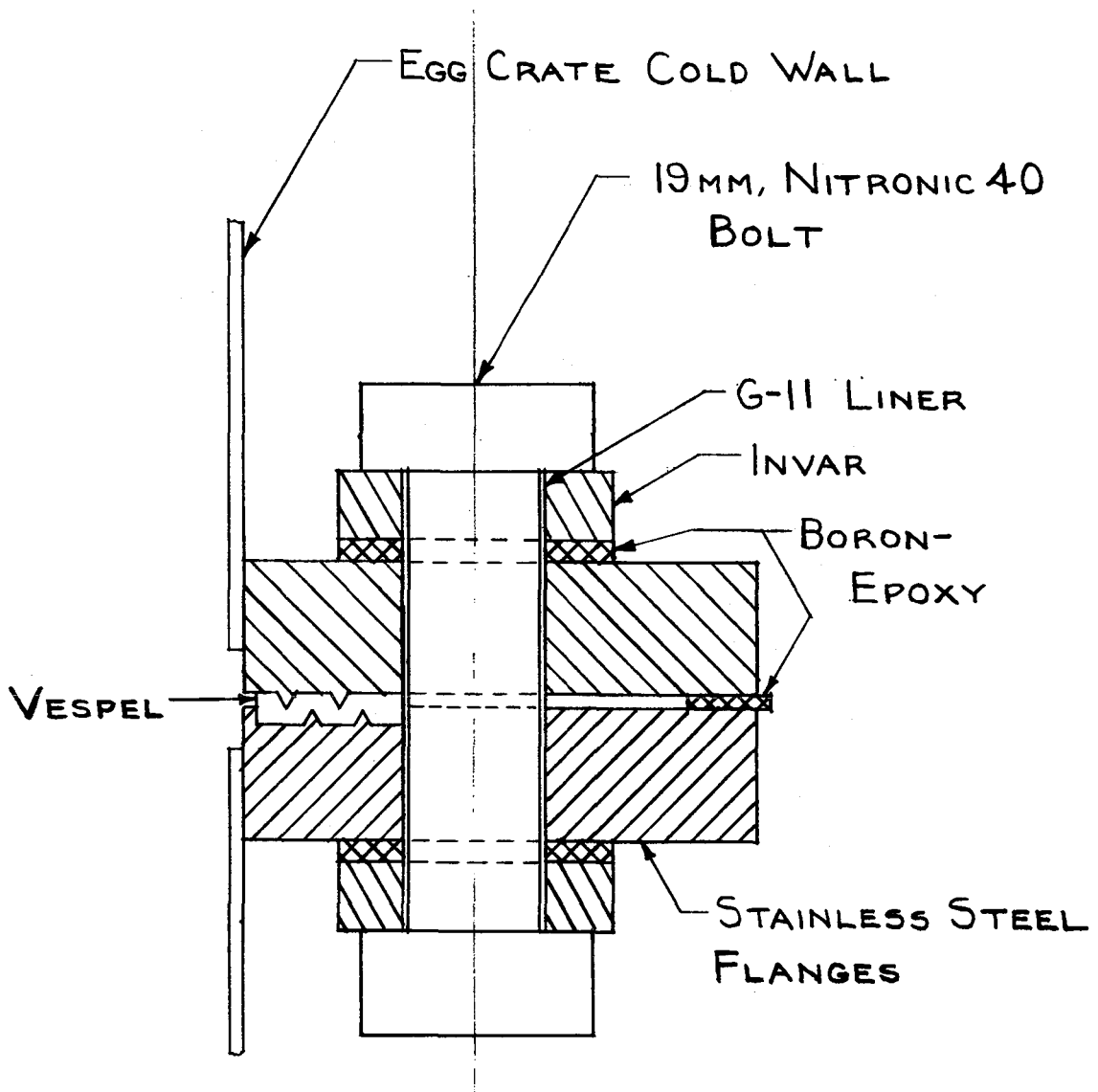
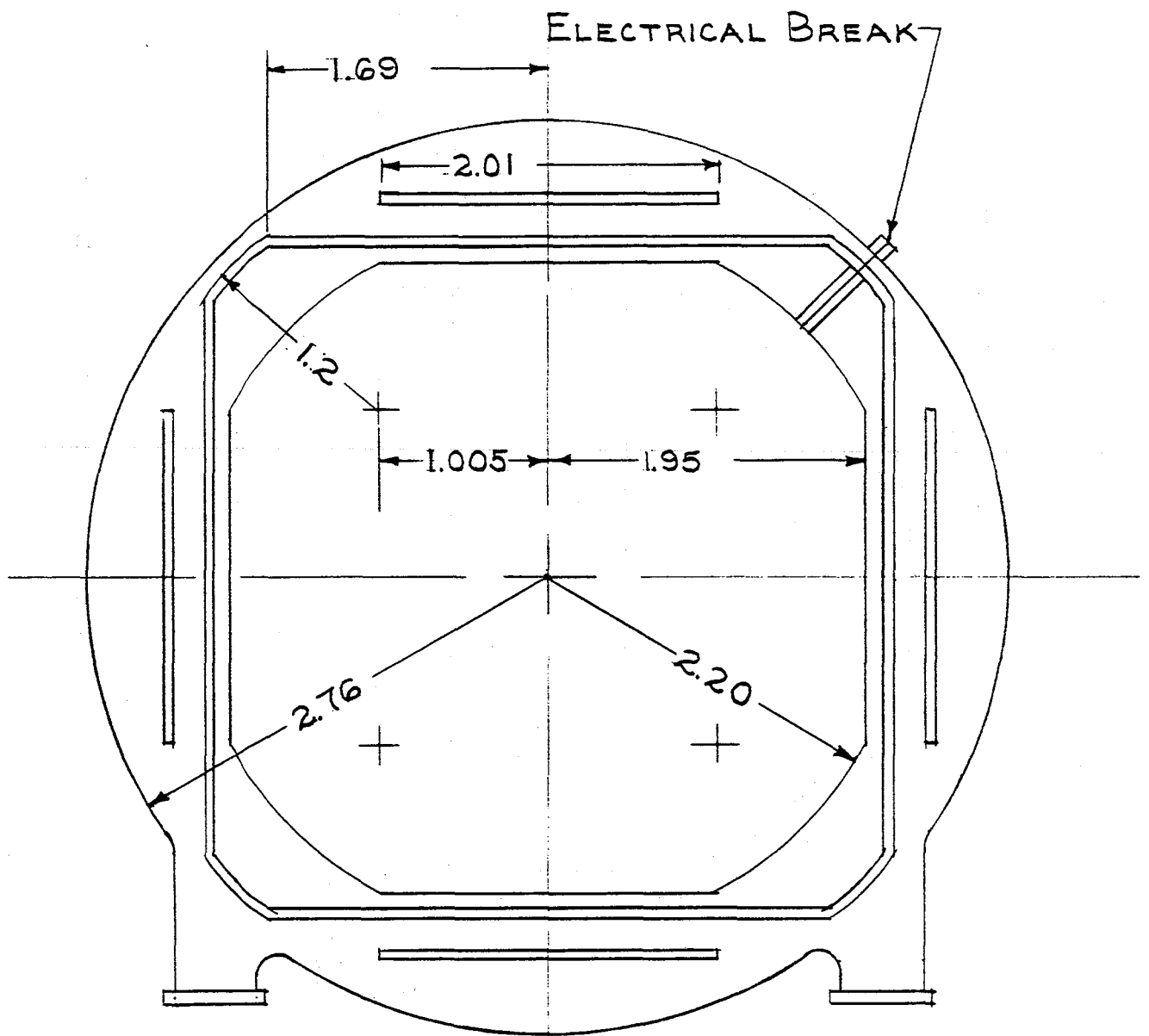
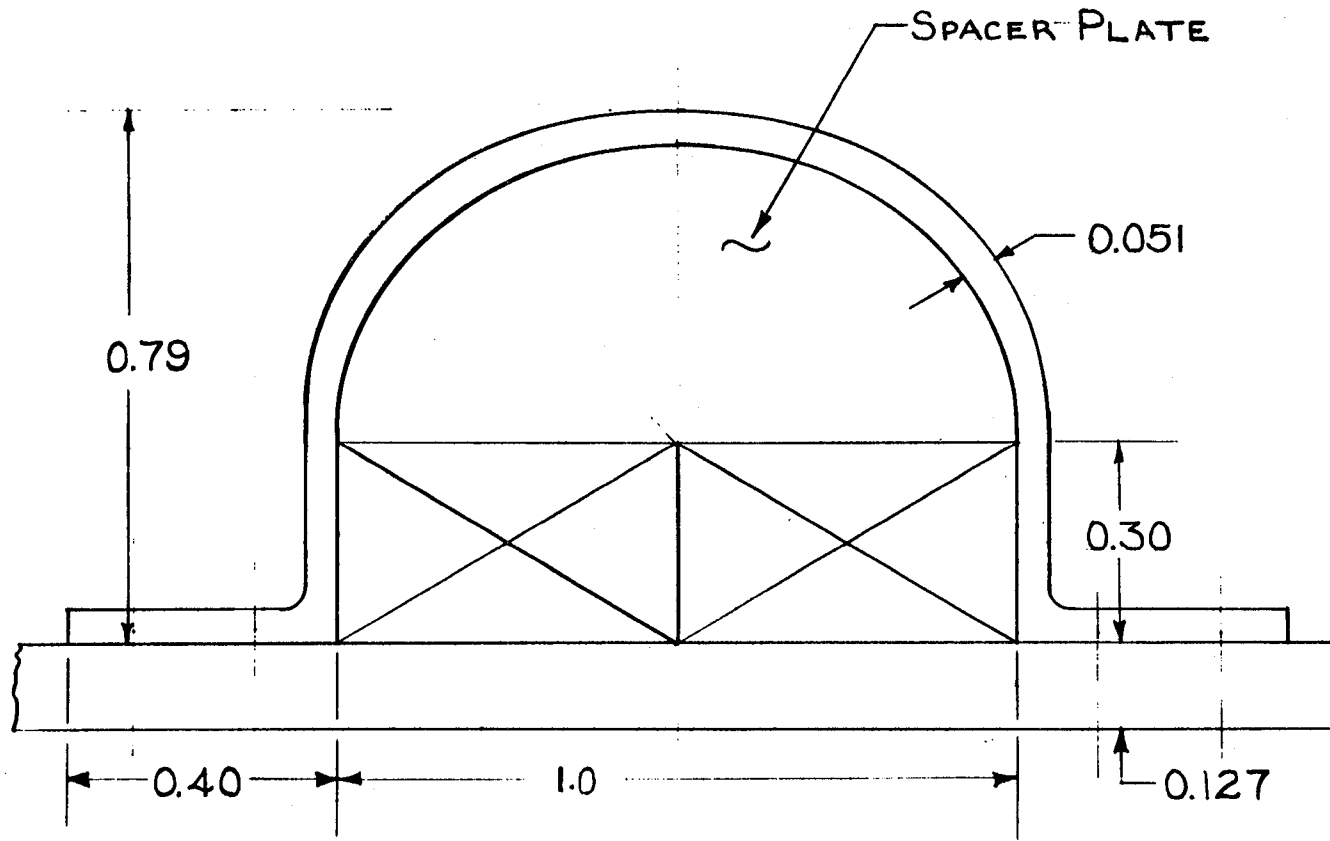


Figure V.5. Egg Crate Electrical Break



Dimensions are in meters.

Figure V.6. End Plate Assembly



Dimensions are in meters.

Figure V.7. Roll Coil Restraint and Structural Stiffener

OFHC Copper--This high quality copper will be used for the liquid nitrogen temperature shields in the egg crate assembly and in the outer cryostat wall. Mechanical properties are not a factor in this application.

Boron-Epoxy--This composite has very high compressive strength and is useful for insulating washers and flange spacers. Allowable compressive stress is in excess of 344.75 MN/m^2 .

Vespel--Vespel is the DuPont trade name for a series of hard fluorocarbon compounds which maintain physical stability when cycled from 4.2 to above 400 K. Vespel is proposed as the sealing material for electrical breaks.

Multilayer Insulation--Multilayer insulation consisting of double aluminized (400 to 500 Angstrom) Mylar interleaved with either glass paper or polyolefin scrim is proposed for the outer portion of the cryostat.

Perlite--Evacuated Perlite powder insulation is effective in cryogenic use. The egg crate assembly would be filled with Perlite.

V.3. Forces and Torques

Forces and torques on each magnet are given in Table III-3 for maximum loadings. Structural calculations assume that these maximum forces occur simultaneously which results in overly conservative design. This is the most feasible approach at present.

V.4. Structural Design

The current structural design is simplified by the decision to separate magnet forces from the cryostat. In this way, both the egg

crate assembly and outer cylindrical portion of the cryostat are designed only to retain helium at a maximum of two atmospheres absolute and not to react other forces except their own dead weight.

The main structural assembly is shown in Figs. V.1 and V.2. It consists of two 304N stainless steel end assemblies (see Fig. V.6) to which are fastened four large epoxy-fiberglass slabs. Edges of the slabs are fixed by four stainless steel longitudinal corner brackets. Span of the slabs is halved by a center epoxy-fiberglass ring and additional longitudinal stiffening is provided by the roll coil restraining tunnels shown in Fig. V.7. The eight identical Y and Z coils are clamped directly to the structural slabs using specially fabricated bolts countersunk into the external surface. Roll coils are mounted on the outside of the slabs using the restraining tunnels of Fig. V.7 to provide clamp forces. Drag coils are wound onto the end assemblies prior to fabrication of the rest of the structure.

Assembly steps for the MSBS include:

1. Wind drag coils on end assembly plates.
2. Assemble end plates, slabs, center ring and corner brackets using bolts and epoxy.
3. Install Y and Z coils.
4. Install roll coils and restraining tunnels.
5. Install complete magnet array and structure into the completed cylindrical outer portion of the cryostat. (Leg stubs may need to be shortened from those shown in Fig. V.6.)
6. Slide the complete egg crate structure into the magnet/structure assembly. Egg crates will be supported off the corner brackets and ID of the drag coils.

7. Install warm and cold end bell assemblies. This is the only assembly process requiring actual fabrication.
8. Install complete wind tunnel test section inside the MSBS unit without loading the egg crate structure.

V.5. Electrical Isolation

Use of predominantly fiberglass-epoxy structure greatly reduces eddy current losses. However, it is still necessary to eliminate significant remaining closed metallic loops. Principal metallic loops are the end assemblies, outer cold shell of the cryostat and the cold wall of the egg crate. Detailed electrical break designs developed for each of these applications are shown in Figs. V.3, V.4 and V.5.

The end plate electrical break concept shown in Fig. V.3 differs from the other two because it is purely structural and does not require vacuum sealing. Thus, this design features a simple G-11 insulating sheet sandwiched between massive flanges. Integrity of the joint is achieved with a combination of 56 mm Nitronic-40 bolts and tapered pins which provide alignment and shear transfer. All surfaces are insulated to prevent electrical leakage and bolts are provided with Invar washers to assure tightness of the joint on cooldown.

Electrical breaks on the outer cold shell and egg crate wall combine vacuum sealing and some structural integrity. The first, Fig. V.4, is more difficult because the 4.83 mm shell to which it is attached is under internal pressure which creates a maximum separating force of 0.626 MN/m. The egg crate wall is simpler because it is under external pressure and the joint (Fig. V.5) is being forced together. Aside from these differing tensile requirements, both breaks are of similar design

in that they utilize sharp triangular ridges which bite into a Vespel sealing strip, have massive flanges to reduce bending, use high modulus boron-epoxy strips at the outer edge to force loads on the Vespel, and shim the Nitronic-40 bolts with substantial Invar washers to make certain that the joints tighten on cooldown. These joints reflect current technology for vacuum/cryogenic seals but still warrant a careful preliminary test program.

V.6. Weight Summary

Estimated weights of MSBS system components are given in Table V-1. The total weight is 210,000 kg \pm 15%, which is 43% less than the 1984 MSBS design. The same support system is used here because its heat leak, 2.4 W, is only 2.5% of the zero load loss.

Table V-1

MSBS System Estimated Weight

Component	Weight
Composite structure	22,290 kg
Stainless steel internal structure	38,080
Outer shell and rings	18,540
Inner cold shell	4,880
End bells	8,440
Egg crate assembly	4,880
Liquid nitrogen shield	2,040
Multilayer insulation	780
Cryostat sub-total	99,930
Helium--30,000 l	3,780
Magnets	80,910
Bolts, magnet clamp plates, miscellaneous	25,380
Total weight	210,000 kg

VI. THERMAL AND CRYOGENIC SYSTEM

VI.1. Cryogenic Concepts

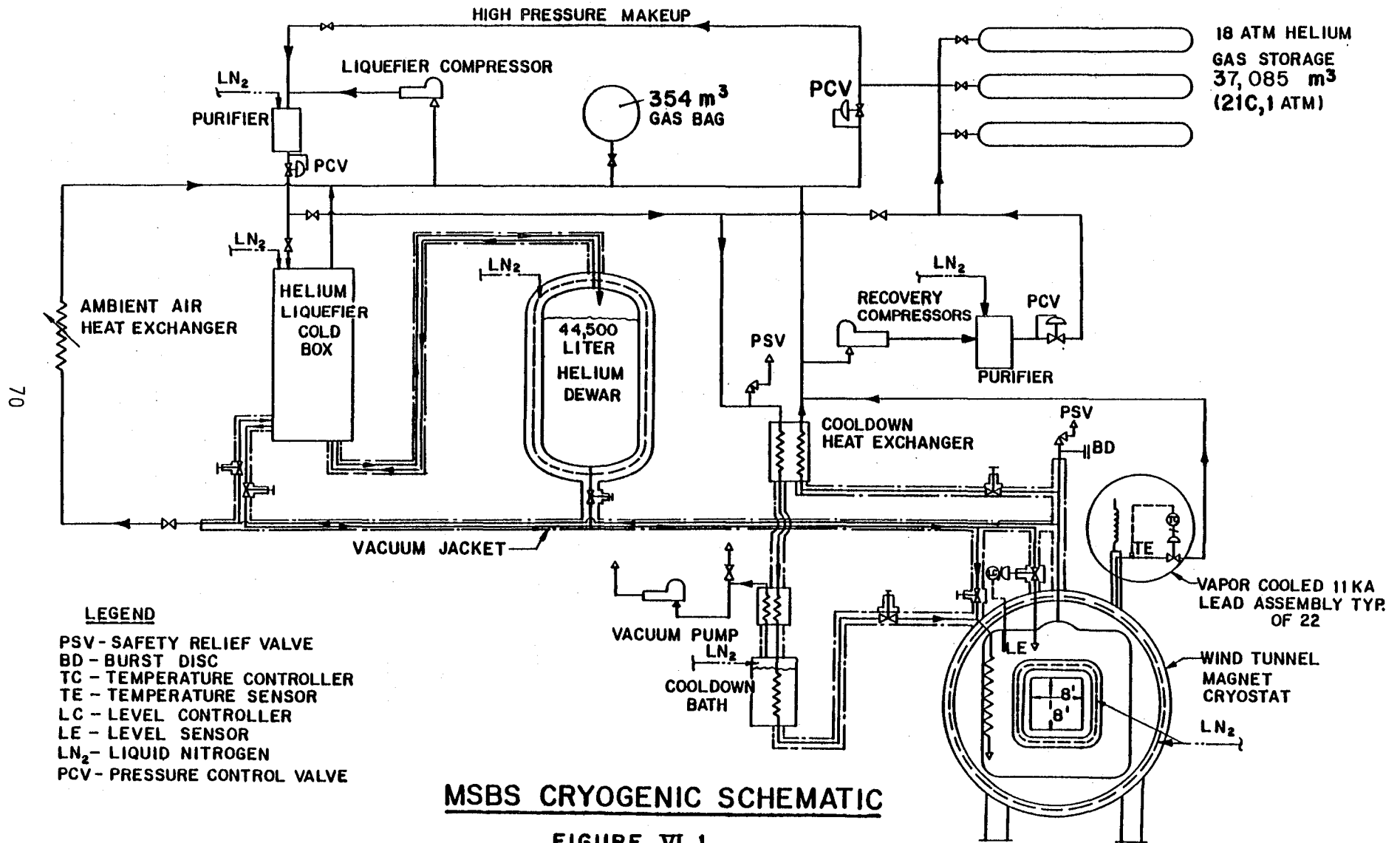
A schematic of the proposed cryogenic system is shown in Fig. VI.1. Major elements of the system include the magnet cryostat, helium liquefier, helium storage dewar, helium recovery compressor, 18 atm. helium gas storage, and a cooldown loop. Design of the system is based on the following criteria:

- Reasonable cooldown time of seven to eight days.
- Adequate liquid storage to fill the magnet cryostat with reserve to meet daily operating deficits.
- Available liquid storage capacity sufficient to empty the cryostat without loss of helium.
- Liquefaction capacity to maintain scheduled operations on a continuous basis.
- Sufficient compressor capacity to handle the maximum planned rate of gas evolution without helium loss.
- Helium gas storage for all of the helium in the system to permit an indefinite shutdown.

Considerations relating to the design and operation of each part of the system are discussed in the following sections.

VI.2. Cryostat Heat Leak

Static heat leak of the cryostat is given in Table VI-1. Over half of the heat leak, 25.4 W, is due to the egg crate assembly which is relatively thin, 0.152 m, and utilizes Perlite insulation which is much less efficient than multilayer. However, multilayer insulation is not



feasible for the cellular structure of the egg crate so the major concern is to make certain that a good fill of Perlite is obtained to avoid radiation heat shorts. Projected accuracy of the static heat leak calculations are -10, +30% for the egg crate and \pm 15% for the 15.2 W balance of the system making the plus side range of 9.9 W, about twice the projected contingency.

Table VI-1

Static Heat Leak and Cryogen Consumption

Item	Heat Leak--W	
	Helium	Nitrogen
Egg Crate Assembly	25.4	430.3
Lead/Vent Stack	6.0	24.0
Outer Cylinder	5.1	90.5
Legs and Braces	2.4	16.8
End Bells	1.7	30.5
Contingency	<u>4.4</u>	<u>57.9</u>
Totals	45.0 W	650.0 W

Helium Consumption--63.5 liters/hour

Nitrogen Consumption--14.5 liters/hour

VI.3. Magnet Power Leads

Each magnet has a pair of leads including one pair for the series roll coils, for a total of twenty-two 11 kA leads. Since there is excess helium vapor available in all operating conditions, the leads are designed to reduce no-load losses. Thus the leads are twice as long as normal and the vapor cooling rate at full load is 0.08 g/s, nearly double the 0.046 g/s/kA optimum rate for standard leads. Without increased cooling, full-load lead losses would be twice normal instead of 46% normal. Reductions in lead losses realized with increased vapor flows are not free because the cold vapor could otherwise return to the refrigerator to increase its capacity. However, at full load more vapor is produced than the refrigerator could accept so excess flow through the leads is the most efficient way to utilize the available vapor cooling. Lead losses presented in Table VI-2 reflect use of all available vapor for the leads at zero and one-fourth load and flows limited to 0.08 g/s/kA at full load.

VI.4. Operating Losses

Combined loss values for magnets, cryostat and leads are given in Table VI-3. These losses determine the size of the cryogenic support system.

Table VI-2
Lead Losses

Magnet Load	Heat Input--W	Helium Loss-- ℓ /h
Zero	53	74.8
1/4	59.3	83.7
Full	110	155.2

Table VI-3

Magnet and Cryostat Operating Losses

Source of Loss	Zero Load W	1/4 Load W	Full Load W
Magnets	0	214.3	522
Structural eddy current	0	50	200
Leads	53	59.3	110
Static heat leak	45	45	45
Conductor joints	0	3.2	51
Totals--W	98	370.9	928
Helium Consumption-- ℓ/h	138.2	523.2	1309.1

In Ref. 2 it was shown that the cryogenic system cost only decreases about 3% if the MSBS is designed to operate on a five-day week cycle in which the weekend is used to catch up on the liquid helium supply. Thus continuous operation seven days per week is chosen.

Assumptions used in sizing the cryogenic system include:

1. Cryostat liquid capacity is 30,000 liters
2. 4000 liters of helium are required for final cooldown of the cryostat from 20 K to 4.2 K
3. Daily operating sequence includes 2 hours at full load, 8 hours at one-fourth load, and 14 hours at zero load.

Size of the refrigerator/liquefier is based on the operating sequence:

Full load--1310 ℓ/h x 2 =	2,620 ℓ
One-quarter load--524 ℓ/h x 8 =	4,192
Zero load--140 ℓ/h x 14 =	<u>1,960</u>
Total daily requirement--	8,772 ℓ
Liquefier size = 8,772 x 1.026*/24h =	375 ℓ/h

The storage dewar is sized by the daily operating deficit and the storage requirements listed above.

Daily Liquid Deficit

Full load--(1310 - 375/1.026)(2) =	1,889 ℓ
One-quarter load--(524 - 375/1.026)(8) =	<u>1,268</u>
Total daily liquid deficit	3,157 ℓ

Required dewar size:

Final cooldown	4,000 ℓ
Fill empty cryostat	30,000
Daily liquid deficit	<u>3,157</u>
Sub-total	37,157
Contingency	<u>7,343</u>
Helium storage dewar size	44,500 ℓ

It is assumed that all of the helium in the system may be converted to gas and stored for an indefinite shutdown. Storage capacity is taken as 10% more than the dewar capacity gas equivalent and 1 atm of the 18 atm storage is considered unavailable. Thus, the volume of gas to be stored, measured at 1 atm and 294.3 K, is

$$V_g = (44,500\ell)(1.1)(0.7576 \text{ m}^3/\ell) = 37,085 \text{ m}^3$$

and the 18 atm physical storage capacity is

$$V_g = 37,085/(18-1) = 2,181.5 \text{ m}^3 = (77,036.4 \text{ ft}^3)$$

Sizing of the recovery compressor is based on the maximum liquid deficit which occurs at full load.

*2.6% allowance for storage and transfer losses.

$$V_R = (1310 \text{ } \ell/\text{h} - 375/1.026) = 944.5 \text{ } \ell/\text{h} \times 0.7576 \text{ m}^3/\ell$$

$$= 715.553 \text{ m}^3/\text{h}.$$

The recovery compressor size is

$$V_R = 715.553/60 = 11.93 \text{ m}^3/\text{min} = (421 \text{ cfm.})$$

This defines the major components of the cryogenic system which are listed in Table VI-4 and illustrated on Figure VI.1.

Table VI-4

Components of MSBS Cryogenic System

Liquefier (ℓ/h).....	375
Storage dewar (ℓ).....	44,500
Recovery compressor (m^3/min).....	11.9
(cfm).....	(421)
System helium charge (m^3).....	37,085
(1 atm, 194.3 K)	
Gas storage at 18 atm (m^3).....	2,182

VI.5. Component Review

All of the cryogenic system components utilize existing technology and commercial experience and there should be no difficulty in locating multiple sources of supply.

Liquefier: The 375 ℓ/h liquefier may not be a catalog size for any manufacturer but it is not large by industry standards and there are three or four American suppliers. Although not analyzed for this study, the helium liquefier is expected to utilize two or, possibly, three gas expanders with final expansion accomplished in a positive displacement wet expander. Overall efficiency of this size of liquefier should be in the range of 17.5 to 20% of Carnot.

Dewar: The helium dewar will probably be a vertical unit with multilayer insulation and an intermediate shield cooled with liquid nitrogen. Loss rate should be in the range of 0.1 to 0.15% per day. Three or four American companies have the technical background and facilities to build this dewar.

Gas Handling: The gas handling system includes the recovery compressor, gas bag and 18 atm storage. The compressor will be a three-stage oil lubricated machine equipped with oil removal components and a small cryogenic purifier so that only high purity helium is stored. The commercially available 354 m³ gas bag provides a low pressure buffer volume for both the liquefier and recovery compressor. When the liquefier is down, the gas bag collects dewar boil-off for periodic pumping into storage by the recovery compressor.

Eighteen atm storage consists of 19 commercial ASME coded propane tanks, each 2.74 m diameter and 20.12 m long. Although space required for this tank farm is appreciable, storage at 18 atm approximately matches the liquefier operating pressure which permits interchangeable use of the recovery and liquefier compressors.

Cooldown System. Only helium is used to cool down the cryostat to avoid the possibility of contamination. The system is designed (see Fig. VI-1) so that both the liquefier and recovery compressors work in parallel for cooldown. Helium flow for cooldown is approximately $33.18 + 11.93 = 45.11$ m³/min and is directed to a special cooldown heat exchanger and liquid nitrogen bath which provide the major refrigeration for cooldown. Liquid nitrogen level in the bath is adjusted for a maximum gas to cryostat temperature difference of 100 K initially to limit thermal shock. As the cooldown proceeds the temperature

difference is reduced until it is less than 5 K at the end. A blower-type vacuum pump is used to reduce the final bath temperature to 65 K in order to get maximum cooling from nitrogen.

Cooling below about 70 K is accomplished by using the liquefier as a cold gas refrigerator. The liquefier is used in this manner until the cryostat is cooled to about 20 K where its enthalpy is only 0.04% of the room temperature value. Cooling from 20 K down to 4.2 K and filling the cryostat is performed in a continuous liquid transfer from the storage dewar. About 4,000 l of liquid helium is required for the final cool-down and 30,000 l used to fill the cryostat.

Liquid and Cold Gas Transfer Lines. Vacuum jacketed helium lines are indicated on Fig. VI-1. The principal VJ line runs from the dewar to the cryostat with a cold gas extension beyond the dewar to the liquefier cold box. This co-axial line consists of a 51 OD x 0.89 mm wall inner liquid line, 5.5 mm radial insulated vacuum space, 63.5 OD x 0.89 mm inner cold gas tube, 101 OD x 1.24 mm outer cold gas tube and a 152.4 OD x 2.77 mm wall (6 IPS, Sch. 5 pipe) warm vacuum jacket. In normal liquid service this line will function as follows:

1. Liquid flows in the inner line at 0.07 to 0.136 atm above the cryostat pressure causing the liquid to be 0.1 to 0.15 K warmer than liquid and gas in the cryostat.
2. Liquid is throttled to cryostat pressure by the flow control valve which drops the temperature with production of a small percentage of flash vapor.
3. Slightly colder vapor returns to the liquefier in the annular gas passage. This cold gas intercepts heat and creates an essentially zero heat leak environment for the inner liquid

line. The purpose of the insulation space between the lines is to prevent the two passages from forming a heat exchanger whenever the return gas is warmer as during cooldown.

Controls and Safety Devices. Since design work to date has been on major functional components, neither the control systems nor safety devices are worked out in detail. As shown in Fig. VI.1., the cryostat is equipped with a level indicator and controller to maintain liquid above the magnets. Because the pressure rating of the egg crate structure is limited, the helium reservoir will be protected by a sensitive pilot-operated relief valve and a parallel burst disc. Each of the 22 magnet leads will be equipped with a flow controller and an overall flow controller will balance lead flows when flows are less than rated 0.88 g/s per lead. Compressors are equipped with bypass circuits and standard over and under pressure switches for automatic unattended operation. As the system detail design evolves, care will be taken to protect all potential isolated cold volumes with thermal relief valves.

VI.6. Cryogenic System Cost Estimate

Estimated cost of the cryogenic system is given in Table VI.5. Costs are escalated 4% from the 1984 MSBS estimates (Ref. 2).

VI.7. Cooldown Analysis

Cooldown is based on the estimated 33.18 m³/min flow from the liquefier compressor plus 11.93 m³/min from the recovery compressor for a total of 45.11 m³/min. This flow rate limits cooldown of the cryostat and it is important to keep the gas to cryostat temperature difference close to 100 K for as long as possible.

Table VI-5

Cryogenic System Cost Estimates

375 l/h helium liquefier	\$1,556,000
Dewar--44,500 l	506,000
18 atm gas storage--2182 m ³	561,000
Recovery compressor--11.93 m ³ /min	169,000
LN ₂ cooldown system	156,000
VJ pipe and valves	104,000
Balance of plant*	156,000
Total	\$3,208,000

*No buildings or civil work.

Estimated time for each of the three phases of cooling is as follows:

300--70 K	130 hours
70--20	36
20--4.2	<u>4</u>
Total	170 hours, 7.1 days

VI.8. General Operating Plan

The operating plan for the cryogenic system from a warm start includes the following steps:

1. Purge and fill the entire system with helium gas.
2. Start flow of liquid nitrogen to the storage dewar shield and to the cryostat shields.
3. Start the liquefier and fill the storage dewar. With a 24-hour allowance for cooldown, it will take about six days to fill the dewar.

4. Cooldown and fill the magnet cryostat. Allow a week for this step.
5. Operate the cryostat as scheduled:
 - a. Whenever gas flow exceeds liquefier capacity the recovery compressor will cycle on to pump gas back to 18 atm storage.
 - b. Liquefier is sized to run continuously when there is liquid in the cryostat and the test regime is followed. For five-day week operation the liquefier would shut down or idle over the weekend.
6. At the end of a wind tunnel operating cycle or at any time the system is to be down more than two weeks, liquid should be transferred back to the dewar and the cryostat allowed to warm up to 78 K by continuing to supply liquid nitrogen to the shields. Restart from this point can be accomplished in about three days.
7. Since the storage dewar will only lose 1,400 to 2,000 liters per month, it should be left cold except for very long shutdowns of three months or more. When the dewar is idling, gas is collected in the gas bag and is pumped back to 18 atm storage about once each week to ten days. Pumping the gas back to storage will take about one-half hour.
8. For long-term shutdown, liquid may be vaporized in the ambient heat exchanger at a rate consistent with the recovery compressor capacity and pumped to high pressure storage.

VI.9. Cryogenic Impact of 1.8 K Operation

Operation at 1.8 K impacts both the cryostat and refrigerator/liquefier. The cryostat must be modified to provide a normal helium reservoir for the leads and a thermally insulated passage between 4.2 and 1.8 K for leads. A heat exchanger for 1.8 K, 12 torr fluid to 1.8 K, 1 atmosphere helium must be provided and piping modifications must be made to limit heat leak into 1.8 K helium. The refrigerator is modified to provide normal helium for lead cooling and intercepts and refrigeration to the 1.8 K, 12 torr heat exchanger. In all cases, enthalpy rise from from 1.8 to 2.0 K for 30,000 liters, $\Delta H = 3.469 \times 10^6$ J, is utilized to extend full power operating time.

If the normal operating sequence is used (2 hours at full power, 8 hours at 1/4 load and 14 hours at idle), the size of the equivalent liquefier is about 845 l/h and its cost is \$2,748,000, an increase of \$1,192,000. Estimated total cost increase for this normal operation option is:

Liquefier addition	\$1,192,000
Cryostat additions:	
Lead dewar & transition	75,000
Heat exchanger	150,000
Specializing & valves	<u>100,000</u>
Total <u>addition</u>	+ \$1,517,000

If 1.8 K operation is a zero cost option, increases in the cryostat and liquefier must match the \$750,000 conductor and magnet saving. This means that the liquefier increase is limited to \$750,000 - \$325,000 =

\$425,000. This buys the equivalent of a 530 l/h liquefier and provides the following performance options:

Full load -- 1.88 hours, or

1/4 load -- 7.83 hours

Either of these options, or a mix (for instance 1 hour at full load + 3.65 hours at 1/4 load) must be followed by a recovery time of 15.2 hours. Thus, several hours of daily operation at 1.8 K could be sustained with this cryogenic system.

VII. COST ESTIMATE

The MSBS cost estimate is \$21,398,000 for a system equivalent to Case 1--Alternate G of NASA CR165917 (Ref. 1). It includes control based on a power amplitude of 0.1% of I_{\max} in all coils simultaneously at a frequency of 10 Hz. The estimates mostly stem from analyses made by MMI. However, several topics have not been addressed by MMI, notably position sensors and the control system, and estimates for these items have been carried forward from NASA CR 165917 and are marked with an asterisk (*) in Table VII-1.

The estimated cost of \$21,398,000 for the MSBS is a reduction of \$8,541,000 or 28.5% from NASA CR 3802 prepared by MMI in 1984. This significant cost reduction is attributed to the following factors:

- * Increased pole strength of the model core magnet by use of a holmium mandrel.
- * Use of $\text{Nd}_{15}\text{Fe}_{77}\text{B}_8$ permanent magnet material in the model wings.
- * Overall reduction in control magnet sizes due to the above factors and a more efficient configuration of the roll coils.
- * Continued better understanding of the MSBS system.
- * More realistic power supply utilization.
- * Structural design to minimize eddy current heating.

Costs presented in Table VII-1 are not contingent on additional analytical or experimental efforts but assume that such work would be accomplished as required. These estimates would be impacted by a future program addressed to some of the key features of the MSBS by more accurately quantifying the design parameters. This work would not

necessarily further reduce the MSBS cost, but it would improve the accuracy of the estimate and validate technical feasibility.

Estimates include 4% escalation of comparable items from 1984 except that structure was based on the same \$10 per fabricated pound used previously. Machines and Tooling, 1.3.2, was reduced from \$1,458,000 to \$1,000,000 because the X, Y and Z coils are much smaller than previously and can be wound on commercially available equipment. This leaves the major portion of the Machines and Tooling budget for design and fabrication of the Roll coil winding fixture.

Table VII-1

MSBS Cost Estimate (Costs in Thousands \$)

1.0	Complete MSBS System		\$21,398
1.1	Preliminary Design Phase		875
1.1.1	System Engineering	\$ 100	
1.1.2	Magnet Preliminary Design	150	
1.1.3	Cryogenics Preliminary Design	60	
1.1.4	Power Supply and Protection Preliminary Design	30	
1.1.5	Position Sensors Preliminary Design	130*	
1.1.6	Control System Preliminary Design	90*	
1.1.7	Support Structure Preliminary Design	140	
1.1.8	Manufacturing Engineering	20	
1.1.9	Quality Control Plan	40	
1.1.10	Preliminary Design Phase Program Management	115	
1.2	Final Design Phase		2,765
1.2.1	System Engineering	150	
1.2.2	Magnet Final Design	300	
1.2.3	Cryogenics Final Design	275	
1.2.4	Power Supply and Protection Final Design	100	
1.2.5	Position Sensors Final Design	420*	
1.2.6	Control System Final Design	350*	
1.2.7	Support Structure Final Design	445	
1.2.8	Manufacturing Engineering	175	
1.2.9	Quality Control and Testing	175	
1.2.10	Final Design Phase Program Management	375	
1.3	Manufacturing, Installation and Checkout Phase		17,758
1.3.1	Engineering Support for Manufacturing, Installation and Checkout	680	
1.3.2	Special Machines and Tooling	1,000	
1.3.3	Manufacturing Z Gradient Coils	381	
1.3.4	Manufacturing Y Gradient Coils	381	
1.3.5	Manufacturing Roll Coils	1,039	
1.3.6	Manufacturing Drag Coils	802	
1.3.7	Model Core Magnet and Cryostat	150	
1.3.8	Cryogenic System	3,198	
1.3.9	Power Supplies and Protection Systems	2,028	
1.3.10	Position Sensors	1,068*	
1.3.11	Control System	1,046*	
1.3.12	Support Structure and Cryostat	2,198	
1.3.13	Quality Control and Testing	175	
1.3.14	Not Used		
1.3.15	Packing and Shipping	250	
1.3.16	Assembly and Installation	1,000	
1.3.17	Checkout and Acceptance Testing	1,012*	
1.3.18	Manufacturing, Installation, Checkout Phase Program Management	1,350	

*These values taken directly from NASA CR 165917 for Case I, Alternate G

VIII. APPENDICES

Appendix A. Magnetic Pole Strength of a Superconducting Solenoid with Holmium Mandrel.

Appendix B. Roll Torque Analysis.

Appendix C. Force and Torque Requirements.

Appendix D. Cross Coupling Analysis.

Appendix E. Optimization of Drag and Roll Coils.

Appendix F. Tunnel Wall Constraints.

APPENDIX A
MAGNETIC POLE STRENGTH OF A SUPERCONDUCTING
SOLENOID WITH HOLMIUM MANDREL

Assume the following superconducting coil nomenclature:

J = gross current density in winding

b = winding outer radius

a = winding inner radius and holmium outer radius

c = holmium inner radius

M_h = holmium magnetization a function of magnetic field

For a long solenoid ($L \gg 2b$), the maximum field at the winding is at the midplane,

$$B_m = \mu_o J (b - a) . \quad \text{A.1}$$

The magnetic pole strength of the winding, Q_m , and of the holmium, Q_h , are

$$Q_m = \pi J (b^3 - a^3)/3, \quad \text{A.2}$$

and
$$Q_h = \pi M_h (a^2 - c^2)/\mu_o . \quad \text{A.3}$$

The total magnetic pole strength is

$$Q = \pi J \left\{ b^3 - \left(b - \frac{B_m}{\mu_o J} \right)^3 \right\} / 3 + \pi M_h \left\{ \left(b - \frac{B_m}{\mu_o J} \right)^2 - c^2 \right\} / \mu_o \quad \text{A.4}$$

APPENDIX B

ROLL TORQUE ANALYSIS

The wing configuration used in this analysis is that of the F16 fighter model. The arrangement of the wing plan form is shown in Figs. B.1 and B.2. Using the non-dimensionalized airfoil coordinates provided by NASA, the cross-sectional area A at any chord of length C is

$$A = 0.02625 C^2 \quad \text{cm}^2 . \quad \text{B.1}$$

At the tip $C = 9.8$ cm and $A = 2.52$ cm² while at the fuselage $C = 43.18$ cm and $A = 48.9$ cm². Actually, the wing begins at $y = 6$ which is the outer radius of the model core and extends to $y = 41$ cm at the tip. The cross-sectional area at any distance y is

$$A(y) = 48.4 - 1.8453 y - 0.0173952 y^2 \quad \text{cm}^2 . \quad \text{B.2}$$

Taking M as the average magnetization in the y direction, it is easy to show that the net torque is

$$T_r = \frac{2}{\mu_0} \{ bMa(b)B_z(b) - aMA(a)B_z + M \int_a^b B_{zR}(y) y dA_y \} \quad \text{B.3}$$

where $a = 0.06$ m, $b = 0.41$ m, and $B_{zR}(y)$ is

$$B_{zR}(y) = B_z(b) \frac{y}{b} .$$

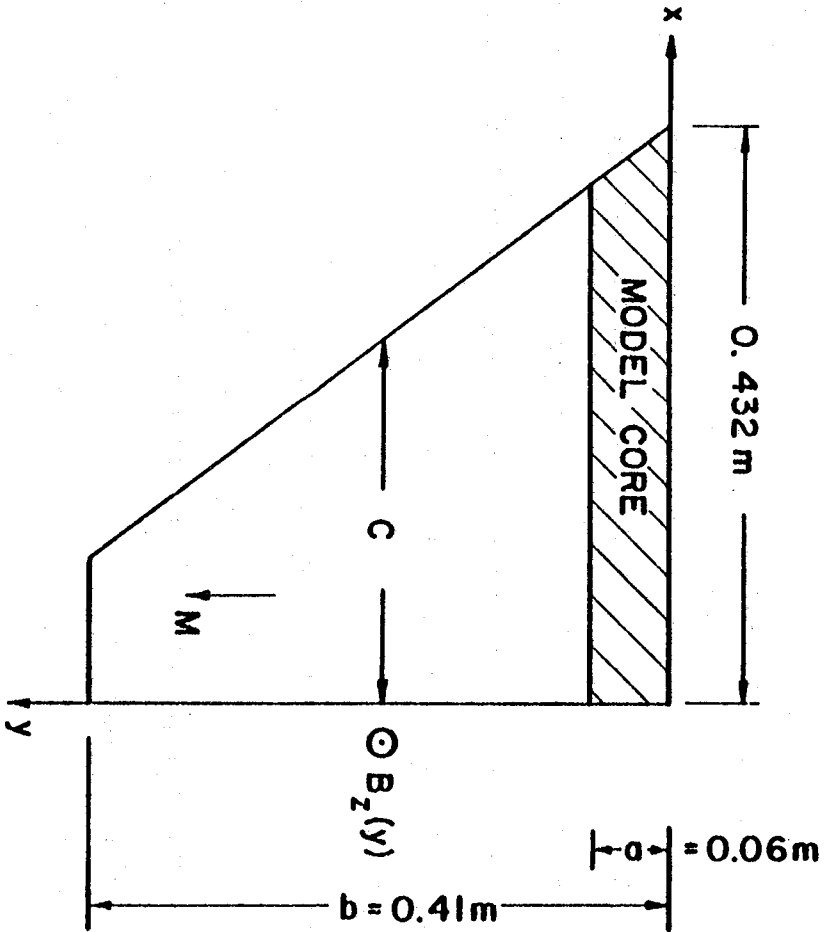


Figure B.1. F16 Wing.

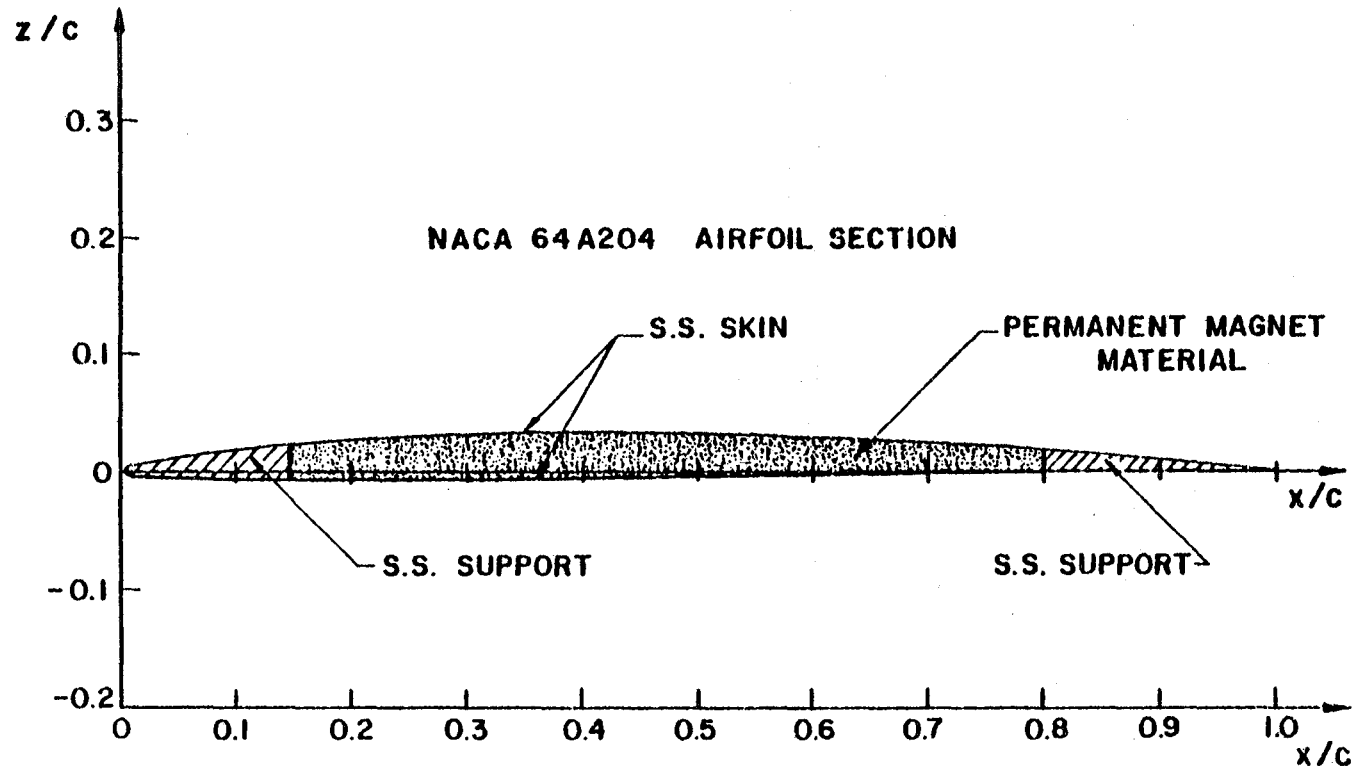


Figure B.2. Wing cross-sectional area at any chord length C showing stainless steel support, skin, and permanent magnet material.

B_z and M are in tesla while distances are in meters and T_r is in Nm.

From the above equations, the magnetic field $B_{zR}(b)$ at the tip of the wing is

$$B_{zR}(b) \cong 4\pi 10^{-4} \frac{T_r(0)}{M},$$

where $T_r(0)$ is the torque at zero roll angle ϕ . To produce the required torque of 141 Nm at $\pm 20^\circ$,

$$T_r(0) = 141 / (\cos^2 20^\circ - \sin^2 20^\circ) = 184 \text{ Nm.} \quad \text{B.6}$$

Equations B.5 and B.6 are used to calculate the roll coil field at wing tips.

APPENDIX C

FORCES AND TORQUE REQUIREMENTS

The requirements for static forces and moments are listed in Table C-1. If the model is replaced by a magnet of a length L and a pole strength Q , then the force in the i^{th} direction for $+ B_i$ at the north pole and $- B_i$ at the south pole (typical of MSBS fields) is

$$F_i = 2Q B_i , \quad \text{C.1}$$

where: F_i = force in the i^{th} direction (N)

Q = model magnet pole strength (Am)

B_i = magnetic field in the i^{th} direction at the core tips (T)

i = x, y, or z.

The magnetic field at the poles of the core, B_i , is the field due to all coils in the i^{th} direction at any position of pitch and yaw.

The pitch and yaw torques are

$$T_p = Q L \delta B_z \cos \alpha , \quad \text{C.2}$$

and
$$T_y = Q L \delta B_y \cos \beta , \quad \text{C.3}$$

where δB_z and δB_y are the difference in B_z and B_y at the two end model tips. δB_z appears in Eq. C.2 because the F_z forces at each end of the pole tip are in the same direction and result in the torque only if one $F_{z1} = Q B_{z1}$ is larger than $F_{z2} = Q B_{z2}$, or $\delta B = |B_{z1} - B_{z2}| > 0$. The pitch and yaw angles are α and β .

Table C-1

MSBS Requirements, 8' x 8' Test Section

A. Static Force Requirements	
Lift	9790 N
Side	1380 N
Drag	4180 N
B. Static Moment Capability	
Pitch	420 Nm
Yaw	140 Nm
Roll	140 Nm
C. Angular Displacement Range	
Angle of Attack (α)	$\pm 30^\circ$
Angle of Sideslip (β)	$\pm 10^\circ$
Angle of Roll (ϕ)	$\pm 20^\circ$
D. Core Dimensions	
Length	75 cm
Diameter	12.7 cm
E. Wing Dimensions	(see Figs. B.1 and B.2 in Appendix B)
F. Dynamic Force Requirements, $\pm 0.1\%$ at 10 Hz	
Lift	± 9.79 N
Side	± 1.38 N
Drag	± 4.18 N

The roll torque at any roll angle ϕ is

$$T_r \cong 2 q b B_{zR} \{ \cos^2 \phi - \sin^2 \phi \}, \quad C.4$$

where q is an equivalent magnetic pole strength of the permanent magnets in the wing tips and $2b$ is the equivalent span. Details of roll torque calculations are provided in Appendix B. B_{zR} is the z component of the magnetic field at the tip of the wing for $\phi = 0$.

APPENDIX D

CROSS COUPLING ANALYSIS

An ideal situation for the MSBS would be for all coils to function independently. Unfortunately this is not possible when the model plane pitches, yaws or rolls. Then there are some minor cross couplings and some major cross couplings. When the model is at zero angle of pitch, yaw and roll, there are no cross couplings between any group of coils with any other group of coils. When the model pitches, yaws or rolls, cross coupling occurs. For larger angles the cross coupling is larger. Hence the largest angle of pitch, $\pm 30^\circ$, will cause the highest mode of cross coupling. The arrangement of magnetic material in the model wings (positive poles are at wing tips while negative poles at fuselage) will result in no roll moment or force from the X, Y or Z coils. Consequently, the R coils suffer no cross coupling from the X, Y or Z coils while the latter suffer from the high R coil field. Therefore, we emphasize the X, Y and Z coils which are subject to cross coupling from the R coil.

Drag Coils (X Coils)

The drag coils have no cross coupling with the R coils because the main current in the R coils is in the x direction which produces no B_x component. When the model pitches, there is cross coupling between the B_x component from the Z coils and the X coil B_x field. This component may be calculated from $\nabla \times B = 0$. Similarly, as the model yaws, there is cross coupling between the B_x component of the Y coils and the X coil B_x field. Unfortunately, these two cross coupling components act

against the required B_x component. At angles α and β in pitch and yaw the B_x component is related to the x, y and z field component of the X, Y and Z coils, respectively, as

$$B_x = B_{x0} \cos \alpha \cos \beta - B_{y0} \sin \beta - B_{z0} \sin \alpha, \quad \text{D.1}$$

where: B_{x0} is the x component due to the X coils at $\alpha = \beta = 0$

B_{y0} is the y component due to the Y coils at $\alpha = \beta = 0$

B_{z0} is the z component due to the Z coils at $\alpha = \beta = 0$.

Z Gradient Coils

When the model pitches or yaws, the total z component at the model tip will be the sum of the z component due to the Z coils, a cross coupling z component from the X coil, and a cross coupling z component from the R coils.

The cross coupling component from the X coil during pitch may be found from $\nabla \cdot B = 0$ and is $+ B_{x0}/2 \sin \alpha$.

When the model core yaws, the model coil tips experience a B_z component field produced by the R coils. This B_z field from the R coils produces a net F_z force (no pitch torque) on the model core. This force is equal to slightly less than one-third of the maximum F_z required on the model. Correction is made by increasing the ampere-meters of the Z coils to balance the undesired z force from the R coils. The undesired B_z component during yaw is related to the z component from the R coils at the wing tips, B_{zR} , as

$$B_z = B_{zR} (L/2b) \sin \beta = A \sin \beta. \quad \text{D.2}$$

where L is the model core length and 2b is the wing span.

The total maximum possible B_z field at angles α and β in pitch and yaw is

$$B_z = B_{z0} \cos \alpha + B_{x0} \frac{1}{2} \sin \alpha - A \sin \beta . \quad D.3$$

In the above equation, cross coupling from the X coils will always strengthen the required B_z component during pitch (positive cross couplings) while the z component from the R coils during yaw may add to or subtract from the net B_z field depending on the angles of roll and yaw.

Y Gradient Coils

There is a positive coupling y component from the X coils equal to

$$(+ \frac{1}{2} \sin \beta) B_{x0} . \quad D.4$$

When the model core pitches, the end tips experience a B_y component from the R coil which translates into a net undesired F_y side force.

The undesired B_y field component is

$$B_y = B_{zR} \frac{L}{2b} \sin \alpha = A \sin \alpha . \quad D.5$$

This y component from the R coils causes a serious cross coupling problem; unfortunately there is no apparent solution except for making the Y gradient coils large enough to take care of this undesired field component.

The total required B_y field at angles of α and β in pitch and yaw is

$$B_y = B_{y0} \cos \alpha \cos \beta + 1/2 B_{x0} \sin \beta - A \sin \alpha . \quad D.6$$

APPENDIX E OPTIMIZATION OF DRAG AND ROLL COILS

E.1 Procedure

The procedure to optimize the ampere meters "IS" of the drag and roll coils is as follows:

- 1) Express the required x-field at the poles of the model magnet due to the drag coils in terms of drag coil design parameters and locations.
- 2) Express the required z-field from the roll coil at the wing tip in terms of roll coil design parameters and locations.
- 3) Write an expression for the total ampere-meters in the drag and roll coils as a function of the dependent variables.
- 4) Write the constraints on the optimization.
- 5) Optimize equation (3) subject to the constraints of (4).

E.2 Magnetic Field Due to Drag Coils at Model's Pole

The field at point Q (Fig. E.1) is

$$B_x = H_o \left[\frac{F(\alpha, \xi_1 + \beta) - F(\alpha, \xi_1 - \beta)}{2F(\alpha, \beta)} - \frac{F(\alpha, \xi_2 + \beta) - F(\alpha, \xi_2 - \beta)}{2F(\alpha, \beta)} \right], \quad (E.1)$$

where

$$\alpha = 1 + \frac{f}{t}$$

$$\beta = \frac{q}{2t}$$

$$\xi_1 = \frac{p + q/2 - z}{t}$$

$$\xi_2 = \frac{p + q/2 + z}{t},$$

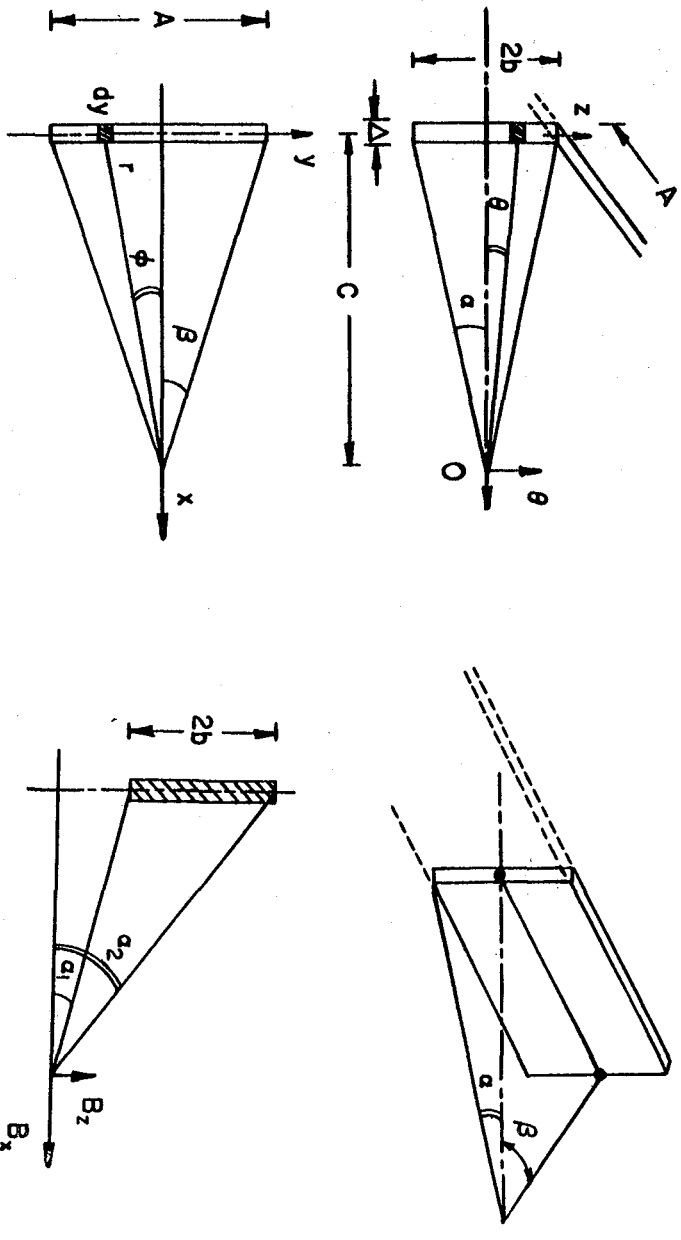


Figure E.1. Field Due to Current Sheet

$$F(\alpha, \beta) = \beta \ln \frac{\alpha + \sqrt{\alpha^2 + \beta^2}}{1 + \sqrt{1 + \beta^2}},$$

and

$$H_o = \mu_o JtF(\alpha, \beta).$$

Substituting in (E.1)

$$B_x = \frac{\mu_o Jt}{2} [F(\alpha, \beta + \xi_1) - F(\alpha, \xi_1 - \beta) - F(\alpha, \xi_2 + \beta) + F(\alpha, \xi_2 - \beta)] \quad (E.2)$$

E.3 Magnetic Field Due to the Roll Coil at Wing Tip

To calculate the magnetic field due to the roll coil, let us first find the field due to a current sheet of thickness Δ , height $2b$, and length A .

For a current element $J\Delta dz$ (Fig. E.2) in the y -direction, the field $d\delta B_z$ at point O is

$$d\delta B_z = \frac{\mu_o J\Delta dz}{4\pi} \cdot \frac{\cos\phi \cos\theta}{r^2} dy,$$

where $r = \frac{c}{\cos\phi}$, $y = c \tan\phi$ and

$$dy = \frac{c}{\cos^2\phi} d\phi.$$

Substituting

$$d\delta B_z = \frac{\mu_o J\Delta \cos\theta dz}{4\pi} \frac{c \cos\phi \cos^2\phi}{\cos^2\phi c^2} d\phi$$

and

$$\delta B_z = \frac{\mu_0 J \Delta \cos \theta}{4\pi c} \int_{-\beta}^{+\beta} \cos \phi \, d\phi$$

$$= \frac{\mu_0 J \Delta \sin \beta}{2\pi c} \cos \theta \, dz .$$

Integrating over length $2b$

$$B_z = \frac{\mu_0 J \Delta \sin \beta}{2\pi c} \int_{-\alpha}^{\alpha} \cos \theta \frac{c}{\cos^2 \theta} \, d\theta ,$$

$$\int_{-\alpha}^{\alpha} \frac{d\theta}{\cos \theta} = \ell n \tan \left(\frac{\pi}{4} + \frac{\theta}{2} \right) \Bigg|_{-\alpha}^{\alpha} = \ell n \frac{\tan(\pi/4 + \alpha/2)}{\tan(\pi/4 - \alpha/2)} = 2 \ell n \frac{1 + \tan(\alpha/2)}{1 - \tan(\alpha/2)} ,$$

or

$$\int_{-\alpha}^{\alpha} \frac{d\theta}{\cos \theta} = \ell n \left(\frac{1 + \sin \theta}{\cos \theta} \right) \Bigg|_{-\alpha}^{\alpha} = \ell n \left(\frac{1 + \sin \alpha}{1 - \sin \alpha} \right) .$$

$$B_z = \frac{\mu_0 J \Delta}{2\pi} \sin \beta \ell n \left(\frac{1 + \sin \alpha}{1 - \sin \alpha} \right) \quad (E-3)$$

where $\alpha = \tan^{-1} \left(\frac{1}{2} \frac{\text{height}}{\text{normal distance}} \right)$ and

$$\beta = \tan^{-1} \left(\frac{1}{2} \frac{\text{length}}{\text{normal distance}} \right) .$$

In general if the current element is enclosed by α_1, α_2 (Fig.

E.3)

$$B_z = \frac{\mu_o J \Delta}{4\pi} (\sin\beta_2 - \sin\beta_1) \int_{\alpha_1}^{\alpha_2} \frac{d\theta}{\cos\theta}, \text{ or}$$

$$B_z = \frac{\mu_o J \Delta}{4\pi} (\sin\beta_2 - \sin\beta_1) \ln \left[\frac{(1+\sin\alpha_2) \cos\alpha_1}{(1+\sin\alpha_1) \cos\alpha_2} \right] \quad (\text{E.4})$$

The field in the x-direction,

$$\delta B_x = \frac{\mu_o J \Delta (\sin\beta_2 - \sin\beta_1)}{4\pi} \sin\theta \, dz,$$

$$B_x = \frac{\mu_o J \Delta (\sin\beta_2 - \sin\beta_1)}{4\pi} \int_{\alpha_1}^{\alpha_2} \sin\theta \frac{c}{\cos^2\theta} d\theta,$$

$$\text{and } B_x = \frac{\mu_o J \Delta}{4\pi} (\sin\beta_2 - \sin\beta_1) \left[\frac{1}{\cos\alpha_2} - \frac{1}{\cos\alpha_1} \right]. \quad (\text{E.5})$$

Now, for the arrangement of roll coil as shown in Fig. (E.4) the z-field due to each coil (1) and (2) at pole tip Q_1

$$B_z = \frac{\mu_o J k}{2\pi} \sin\beta \ln \left[\frac{1+\sin\alpha}{1-\sin\alpha} \right].$$

Substituting for

$$J = \frac{I}{kg}$$

where I = current flowing in one conductor

$$B_{z1} = \frac{\mu_0 I}{2\pi g} \sin\beta_1 \ln \left[\frac{1+\sin\alpha_1}{1-\sin\alpha_1} \right], \quad B_{z2} = -\frac{\mu_0 I}{2\pi g} \sin\beta_2 \ln \left[\frac{1+\sin\alpha_2}{1-\sin\alpha_2} \right].$$

For coil (1) at Q_1

$$\beta_1 = \tan^{-1} \left(\frac{j}{2(\ell-y+k/2)} \right) \quad \alpha_1 = \tan^{-1} \left(\frac{g}{\ell-y+k/2} \right)$$

For coil (2) at Q_1

$$\beta_2 = \tan^{-1} \left[\frac{j}{2(\ell+y+k/2)} \right] \quad \alpha_2 = \tan^{-1} \left(\frac{g}{\ell+y+k/2} \right)$$

For coil (3) at Q_1

$$B_{z3} = \frac{\mu_0 I}{2\pi g} \sin\beta_3 \left[\frac{1}{\cos\alpha_4} - \frac{1}{\cos\alpha_3} \right]$$

For coil (4) at Q_1

$$B_{z4} = \frac{\mu_0 I}{2\pi g} \sin\beta_4 \left[\frac{1}{\cos\alpha_6} - \frac{1}{\cos\alpha_5} \right]$$

$$\beta_3 = \beta_4 = \tan^{-1} \left[\frac{j}{2(\ell+k/2)} \right]$$

$$\alpha_3 = \alpha_5 = \tan^{-1} \left[\frac{y-g}{\ell+k/2} \right]$$

$$\alpha_4 = \alpha_6 = \tan^{-1} \left[\frac{y+g}{\ell+k/2} \right]$$

Total z-field at Q₁, $B_z = B_{z1} - B_{z2} + 2B_{z3}$

$$B_z = \frac{\mu_0 Jk}{2\pi} \left[\sin\beta_1 \ell n \left(\frac{1+\sin\alpha_1}{1-\sin\alpha_1} \right) - \sin\beta_2 \ell n \left(\frac{1+\sin\alpha_2}{1-\sin\alpha_2} \right) + 2\sin\beta_3 \left(\frac{1}{\cos\alpha_4} - \frac{1}{\cos\alpha_3} \right) \right] \quad (\text{E.6})$$

E.4 Total Ampere Meters in the Drag and Roll Coils

The ampere-meters of the two drag coils is

$$IS_x = 2\pi(2t + f) Jqf, \quad (\text{E.7})$$

where J is the current density

t, f, q are as shown in Fig. E.3.

The ampere meters in the roll coil are

$$IS_r = 4(2j + 2\pi r_{c1} + \pi r_{c2}) Jkg,$$

where j, k, g are as shown in Fig. E.2.

For $r_{c1} = 0.5 \text{ m}$,
 $r_{c2} = 1.2 \text{ m}$ and
 $J = \text{current density, we get}$

$$IS_r = (8j + 27.646) \text{ Jkg}$$

$$\text{and } IS_{\text{total}} = 2\pi(2t + f) Jqf + (8j + 27.646) \text{ Jkg} . \quad (\text{E.8})$$

E.5 Optimization Constraints

The constraints on the optimization are as follows:

- (1) For the roll coil $B_z = \text{constant} = F_z/Q_1$
- (2) For the drag coils $B_x = \text{constant} = F_x/Q_2$
- (3) The distance $y = \text{constant} = 0.41 \text{ m}$
- (4) The distance $z = \text{constant} = 0.35 \text{ m}$
- (5) The distance $l = \text{constant} = 2.204 \text{ m}$
- (6) The current density $J = \text{constant}$
- (7) The distance $t = \text{constant} = 2.257 \text{ m}$

E.6 Optimization

To carry out the optimization, let us recall the equations for the magnetic field due to the drag coils,

$$B_x = \frac{\mu_0 Jt}{2} F_2 (\alpha, \beta, \xi_1, \xi_2) , \quad (\text{E.9})$$

where

$$F_2(\alpha, \beta, \xi_1, \xi_2) = F_3(\alpha, \xi_1 + \beta) - F_3(\alpha, \xi_1 - \beta) \\ - F_3(\alpha, \xi_2 + \beta) + F_3(\alpha, \xi_2 - \beta)$$

$$F_3(\alpha, \beta) = \beta \ln \frac{\alpha + \sqrt{\alpha^2 + \beta^2}}{1 + \sqrt{1 + \beta^2}} .$$

Rearranging (E.9)

$$t F_2(\alpha, \beta, \xi_1, \xi_2) = \frac{2B}{\mu_o J} = \text{constant} . \quad (\text{E.10})$$

In the same manner, recall the equation for the magnetic field due to the roll coil

$$B_z = \frac{\mu_o Jk}{2\pi} [F_1(\alpha_1, \alpha_2, \alpha_3, \beta_1, \beta_2, \beta_3)] \quad (\text{E.11})$$

where F_1 is as shown in equation (E.6).

Rearranging Equation (E.11)

$$kF_1(\alpha_1, \alpha_2, \alpha_3, \beta_1, \beta_2, \beta_3) = \frac{2\pi B_z}{\mu_o J} = \text{constant} \quad (\text{E.12})$$

A computer program is used to minimize equation (E.8) subject to the conditions of equations (E.11) and (E.12).

APPENDIX F

TUNNEL WALL CONSTRAINTS

The 10 Hz requirement for dynamic field control requires that a 10 Hz field variation must be transmitted through intervening walls. In NASA CR-165917[1] this problem was approached by estimating the time constants for field diffusion through the intervening wall. The intervening wall was modeled as an infinite cylinder between the magnet system and the airplane model. Table E-1 reproduces the field diffusion chart with an additional entry for the presently planned MMI low temperature 2 mm thick stainless steel wall.

If the test section has a time constant comparable to $\tau = 0.1$ sec then severe field wave form distortion results. Note that the MMI wall thickness of 2 mm has a time constant about 1/3000 of the field driving time constant and would produce no distortion.

A similar conclusion can be drawn from skin depth δ which measures depth of penetration of an incident wave. The skin depth is the distance within a conductor at a point at which the amplitude of the field vector is equal to $1/e = 0.3679$ of its value at the surface.

$$\begin{aligned}\delta &= (2\rho/\mu\omega)^{1/2} \\ &= 36 f^{-1/2} \text{ cm for S.S. at low temperature} \\ &= 11.4 \text{ cm at 10 Hz.}\end{aligned}$$

A wall 2 mm thick is almost transparent at 10 Hz and quite transparent for control frequencies up to 200 Hz.

Table F-1

Time Constants for Field Diffusion Through Dewar Walls

8' x 8' Test Section

	<u>MMI Design</u>	<u>Design of Ref. 1</u>		
Wall Thickness	2 mm	25.4 mm	50.8 mm	76.2 mm
Stainless Steel*	0.0000315 sec	0.005 sec	0.02 sec	0.045 sec
Characteristic time at 10 Hz			$\tau \sim 1/f = 0.1 \text{ sec}$	

* $\rho = 50 \times 10^{-8} \Omega\text{m}$ at low temperature.

[The page contains extremely faint and illegible text, likely bleed-through from the reverse side of the document. The text is arranged in several columns and is too light to transcribe accurately.]

1. Report No. NASA CR-3937		2. Government Accession No.		3. Recipient's Catalog No.	
4. Title and Subtitle MAGNETIC SUSPENSION AND BALANCE SYSTEM ADVANCED STUDY				5. Report Date October 1985	
				6. Performing Organization Code	
7. Author(s) R. W. Boom, Y. M. Eyssa, G. E. McIntosh, and M. K. Abdelsalam				8. Performing Organization Report No.	
9. Performing Organization Name and Address Madison Magnetics, Inc. 216 Walnut Street Madison, Wisconsin 53705				10. Work Unit No.	
				11. Contract or Grant No. NAS1-17931	
12. Sponsoring Agency Name and Address National Aeronautics and Space Administration Washington, D.C. 20546				13. Type of Report and Period Covered Contractor Report 12/84 to 6/85	
				14. Sponsoring Agency Code 505-31-53-10	
15. Supplementary Notes Langley Technical Monitor: Richmond P. Boyden Final Report					
16. Abstract An improved compact design for a superconducting magnetic suspension and balance system for an 8 ft. x 8 ft. transonic wind tunnel is developed. The original design of an MSBS in NASA CR-3802 utilized 14 external superconductive coils and a superconductive solenoid in the airplane test model suspended in a wind tunnel. The improvements are in the following areas: test model solenoid options, dynamic force limits on the model, magnet cooling options, structure and cryogenic designs, power supply specifications, and cost and performance evaluations. The improvements are: MSBS cost reduction of 28%, weight reduction of 43%, magnet system ampere-meter reduction of 38%, helium liquefier capacity reduction by 33%, magnet system stored energy reduction by 55%, AC loss to liquid helium reduced by 76%, system power supply reduced by 68%, test coil pole strength increased by 19%, wing magnetization increased by 40%, and control frequency limit increased by 200% from 10 Hz to 30 Hz. The improvements are due to: magnetic holmium coil forms in the test model, better rare earth permanent magnets in the wings, fiberglass-epoxy structure replacing stainless steel, better coil configuration, and new saddle roll coil design.					
17. Key Words (Suggested by Author(s)) Magnetic suspension Magnetic balance Superconducting magnets Wind tunnel balance			18. Distribution Statement Unclassified - Unlimited Subject Category 09		
19. Security Classif. (of this report) Unclassified		20. Security Classif. (of this page) Unclassified		21. No. of Pages 126	22. Price A07

End of Document